

Cyclic and secular variation in the temperatures and radii of extreme helium stars

C. Simon Jeffery,^{1,2} Rhaana L. C. Starling,^{1,2}★† Philip W. Hill²‡ and Don Pollacco^{2,3}

¹Armagh Observatory, College Hill, Armagh BT61 9DG

²Department of Physics and Astronomy, University of St Andrews, St Andrews, Fife KY16 9SS

³Department of Physics, The Queen's University of Belfast, Belfast BT7 1NN

Accepted 2000 August 25. Received 2000 August 1; in original form 1999 December 9

ABSTRACT

The ultraviolet properties of 17 extreme helium stars have been examined using 150 *IUE* spectra. Combining short-wave and long-wave image pairs and using a grid of hydrogen-deficient model atmospheres and a χ^2 minimization procedure, 70 measurements of effective temperature (T_{eff}), angular diameters (θ) and interstellar extinction (E_{B-V}) were obtained. In most cases, these were in good agreement with previous measurements, but there are some ambiguities in the case of the hotter stars, where the solutions for T_{eff} and E_{B-V} become degenerate, and in the case of the cooler stars with large E_{B-V} , where the total flux is no longer dominated by the ultraviolet.

The behaviour of 12 helium stars was examined over an interval exceeding 10 yr. The surfaces of four stars (HD 168476, HD 160641, BD $-9^{\circ}4395$ and BD $-1^{\circ}3438$) were found to be heating at rates between 20 and 120 K yr^{-1} , in remarkable agreement with theoretical predictions. This result provides the first direct evidence that extreme helium stars are helium shell-burning stars of up to $\sim 0.9 M_{\odot}$ contracting towards the white dwarf sequence. Low-luminosity helium stars do not show a detectable contraction, also in agreement with theory, although one, BD $+10^{\circ}2179$, may be expanding.

The short-term behaviour of three variable helium stars (PV Tel variables: HD 168476, BD $+1^{\circ}4381$, LS IV $-1^{\circ}2$) was examined over a short interval in 1995. All three showed changes in T_{eff} and θ on periods consistent with previous observations. Near-simultaneous radial velocity (v) measurements were used to establish the total change in radius, with some reservations concerning the adopted periods.

Subsequently, measurements of the stellar radii and distances could be derived. With T_{eff} and surface gravities established previously, stellar luminosities and masses were thus obtained directly from observation. In the case of HD 168476, the mass is $0.94 \pm 0.68 M_{\odot}$. Assuming a similar gravity for LS IV $-1^{\circ}2$ based on its neutral helium line profiles, its mass becomes $0.79 \pm 0.46 M_{\odot}$. The θ amplitude for BD $+1^{\circ}4381$ appears to be overestimated by the *IUE* measurements and leads to a nonsensical result. These first direct measurements of luminous extreme helium star masses agree well with previous estimates from stellar structure and pulsation theory.

Key words: stars: chemically peculiar – stars: evolution – stars: fundamental parameters – stars: oscillations – stars: variables: other – ultraviolet: stars.

★ E-mail: csj@star.arm.ac.uk

† Present address: Mullard Space Science Laboratory, Dorking, Surrey RH5 6NT.

‡ Phil Hill died on 1999 May 15. Phil carried out a preliminary survey of the data presented here (Hill & Jeffery 1996), but never saw the final results. His co-authors wish to record their appreciation of Phil's career-long contribution to the science of extreme helium stars and the enthusiasm for astronomy with which he infected all who had the privilege to know him.

1 INTRODUCTION

1.1 Extreme helium stars

As a simple consequence of their energy budget, the evolution of luminous blue stars invariably occurs on time-scales of a few hundred to a few thousand years – extreme helium stars can be no exception. These rare stars have luminosity-to-mass ratios $L/M \sim 10^4$ (in solar units). Their surfaces are predominantly

Table 1. The *IUE* observations of extreme helium stars.

Star	Date	LW image	Exp. (s)	JD	SW image	Exp. (s)	JD
HD 124448	79/01/01	LWR 03347	180	244 3874.884	SWP 03769	180	244 3874.906
					SWP 03770	360	244 3875.148
	79/07/13	LWR 05033	115	244 4068.224	SWP 05789	115	244 4068.219
	93/07/08	LWP 25875	180	244 9177.351	SWP 48067	360	244 9177.344
HD 144941	80/01/19	LWR 06703	120	244 4258.058	SWP 07696	119	244 4258.086
HD 160641	79/06/26	LWR 04855	150	244 4050.922	SWP 05635	309	244 4050.915
	79/07/14–15	LWR 05051	150	244 4069.569	SWP 05800	180	244 4069.465
					SWP 05801	300	244 4069.576
	80/08/08	LWR 08467	150	244 4460.28	SWP 09741	181	244 4460.301
	83/05/14	LWR 15936	150	244 5468.531	SWP 19976	180	244 5468.538
	83/05/14	LWR 15937	150	244 5468.578	SWP 19977	330	244 5468.582
	83/05/14	LWR 15939	150	244 5468.649	SWP 19978	330	244 5468.643
	83/05/14	LWR 15940	150	244 5468.695	SWP 19979	330	244 5468.688
	83/05/14	LWR 15941	150	244 5468.741	SWP 19980	330	244 5468.735
	83/05/14	LWR 15942	150	244 5468.788	SWP 19981	330	244 5468.781
	94/04/26	LWP 27995	180	244 9468.585	SWP 50627	390	244 9468.591
HD 168476	79/07/13	LWR 05032	70	244 4068.124	SWP 05787	40	244 4068.129
	80/03/19	LWR 07247	595	244 4318.186	SWP 08300	666	244 4318.207
					SWP 08301	1442	244 4318.251
	93/07/08	LWP 25872	240	244 9176.613	SWP 48062	600	244 9176.598
	95/05/02	LWP 30588	180	244 9839.503	SWP 54562	600	244 9839.51
	95/05/05	LWP 30615	180	244 9842.517	SWP 54610	600	244 9843.501
	95/05/9–10	LWP 30658	180	244 9847.496	SWP 54648	600	244 9847.506
	95/05/15	LWP 30703	180	244 9852.514	SWP 54680	600	244 9852.525
	95/05/19	LWP 30728	180	244 9856.592	SWP 54705	600	244 9856.6
	95/05/22–23	LWP 30750	180	244 9859.514	SWP 54733	600	244 9860.522
	95/05/28	LWP 30788	180	244 9865.6	SWP 54780	600	244 9865.607
HD 225642	81/08/26	LWR 11418	360	244 4843.195	SWP 14820	900	244 4843.207
	93/07/07	LWP 25869	150	244 9176.362	SWP 48059	2099	244 9176.342
BD +37°1977	78/05/30	LWR 01584	242	244 3659.388	SWP 01672	130	244 3659.345
	78/10/31	LWR 02779	60	244 3813.204	SWP 03196	40	244 3813.179
	79/01/05	LWR 03389	200	244 3878.767	SWP 03808	194	244 3878.755
	79/11/28	LWR 06250	52	244 4205.82	SWP 07247	32	244 4205.837
	80/04/24	LWR 07601	182	244 4354.467	SWP 08823	121	244 4354.456
	94/04/25	LWP 27989	75	244 9467.712	SWP 50622	35	244 9467.707
BD +10°2179	79/11/28	LWR 06249	100	244 4205.76	SWP 07246	300	244 4205.767
	94/04/25	LWP 27988	140	244 9467.632	SWP 50621	200	244 9467.627
BD +1°4381	79/07/13	LWR 05036	240	244 4068.493	SWP 05794	900	244 4068.504
	79/07/14	LWR 05037	480	244 4068.522	SWP 05795	2100	244 4068.555
	93/07/08	LWP 25877	240	244 9177.469	SWP 48068	1800	244 9177.485
	95/05/02	LWP 30589	240	244 9839.586	SWP 54563	1800	244 9839.571
	95/05/06	LWP 30616	240	244 9843.586	SWP 54611	1800	244 9843.571
	95/05/10	LWP 30659	240	244 9847.589	SWP 54649	1800	244 9847.563
	95/05/15	LWP 30704	240	244 9852.595	SWP 54681	1800	244 9852.576
	95/05/19	LWP 30727	240	244 9856.533	SWP 54704	1800	244 9856.518
	95/05/23	LWP 30751	240	244 9860.592	SWP 54734	1800	244 9860.601
		95/05/28	LWP 30787	240	244 9865.535	SWP 54779	1800
BD −1°3438	79/07/10	LWR 04999	300	244 4065.165	SWP 05763	450	244 4065.158
	79/07/14	LWR 05040	720	244 4068.696	SWP 05797	1800	244 4068.679
	82/05/26	LWR 13319	3000	244 5116.189	SWP 17049	7200	244 5116.127
	94/04/26	LWP 27996	2400	244 9468.663	SWP 50628	12900	244 9468.755
		LWP 27997	2099	244 9468.728			
BD −9°4395	79/07/13	LWR 05034	150	244 4068.347	SWP 05791	70	244 4068.342
	79/07/16	LWR 05061	325	244 4070.740	SWP 05812	900	244 4070.752
	93/07/07	LWP 25870	270	244 9176.459	SWP 48060	900	244 9176.431
CoD −46°11775	80/08/07	LWR 08454	480	244 4458.607	SWP 09713	1800	244 4458.624
	81/08/21	LWR 11394	480	244 4838.04	SWP 14788	1498	244 4838.014
	94/04/25–27	LWP 28001	600	244 9469.596	SWP 50623	3000	244 9467.784
				SWP 50624	2700	244 9467.851	
CoD −48°10153	79/07/15	LWR 05052	1800	244 4069.63	SWP 05802	1020	244 4069.652
	81/08/21–25	LWR 11397	1800	244 4838.197	SWP 14811	13500	244 4842.016

Table 1 – continued

Star	Date	LW image	Exp. (s)	JD	SW image	Exp. (s)	JD
LSIV +6°2	89/04/23	LWP 15400	360	244 7640.375	SWP 36075	300	244 7640.382
					SWP 36076	600	244 7640.439
LSIV −1°2	80/08/07	LWR 08455	1800	244 4458.682	SWP 09714	4200	244 4458.721
	94/04/24	LWP 27979	2400	244 9466.61	SWP 50618	15300	244 9466.729
		LWP 27980	2100	244 9466.707			
	95/05/02	LWP 30590	2100	244 9839.65	SWP 54564	9900	244 9839.725
	95/05/06	LWP 30617	2100	244 9843.645	SWP 54612	10200	244 9843.722
	95/05/10	LWP 30660	2100	244 9847.662	SWP 54650	8280	244 9847.735
	95/05/15	LWP 30705	2100	244 9852.774	SWP 54682	8700	244 9852.701
95/05/19	LWP 30729	2100	244 9856.664	SWP 54706	8820	244 9856.732	
LSIV −14°109	80/08/08	LWR 08466	2100	244 4459.876	SWP 09732	1500	244 4459.9
	82/05/26	LWR 13322	3600	244 5116.371	SWP 17052	8280	244 5116.445
	94/04/27	LWP 28002	3600	244 9469.69	SWP 50632	12180	244 9469.714
		LWP 28003	1800	244 9469.768			
LSS 4357	82/09/22–23	LWR 14231	1200	244 5234.819	SWP 18070	4200	244 5235.718
	89/04/23	LWP 15399	4620	244 7640.303	SWP 36074	16500	244 7640.174
LSS 5121	89/04/23	LWP 15402	5100	244 7640.504	SWP 36073	7860	244 7639.985

helium, with a few per cent of carbon and nitrogen and, in general, a negligible contamination by hydrogen. They are almost certainly of low mass. The majority show small-amplitude variations on time-scales of 1–20 d or more, and should correctly be classified as PV Tel variables.

1.2 Evolution and secular changes

The principal question posed by the extreme helium stars is that of their evolutionary origin. Two principal hypotheses have emerged, the chief difference being whether the progenitor is a single or a binary white dwarf. The general properties of both hypotheses are outlined elsewhere (e.g. Saio & Jeffery 2000) and are here simply referred to as the ‘late thermal pulse’ (LTP) model (Iben et al. 1983) and the ‘merged binary white dwarf’ (MBWD) model (Webbink 1984; Iben & Tutukov 1985).

Both hypotheses involve the ignition of a helium-burning shell in an electron-degenerate star, followed by the expansion of the stellar envelope to giant dimensions and then a contraction, once again, to the white dwarf sequence. The expansion phase is thought to take place on the dynamical time-scale, from a few weeks to a few years, whilst the contraction will be on a thermal time-scale (thousands of years).

Examples of stars with both evolutionary histories have been proposed. It has been argued that the rapid expansions observed in V4334 Sgr, FG Sge and V605 Aql are due to a late thermal pulse (or final helium-shell flash: Iben 1984; Seitter 1987; Duerbeck et al. 1997). Some authors have gone on to suggest that, since FG Sge and V4334 Sgr share some properties also shown by the hydrogen-deficient R CrB stars, at least some of the latter are also LTP stars. On the other hand, Saio & Jeffery (2000) have shown that the subluminescent helium star V652 Her could be the consequence of a merger between two helium white dwarfs.

In both the LTP or MBWD cases, the structure of the stellar core – the degenerate region below the helium-burning shell – depends on its previous history and may be reflected in its subsequent evolution. For example, to first order, the luminosity of the helium-burning shell depends on the mass and radius of the

core (Jeffery 1988; Saio 1988). Similarly, the contraction rate of a shell-burning helium giant depends on the luminosity (Saio 1988), the most luminous stars contracting the most quickly. Therefore, if it were possible to plot the evolution of any of these stars in terms of luminosity and radius as a function of time, it would provide an invaluable diagnostic of stellar evolution.

Being hot, extreme helium stars emit principally in the ultraviolet. In the absence of hydrogen, the influence of line blocking on the distribution of flux in the emergent spectrum is highly exaggerated. Line blocking in the ultraviolet comes principally from neutral and singly ionized iron-group elements, and is very sensitive to temperature between 10 000 and 20 000 K. Furthermore, the redistribution of flux caused by line blocking leads to back-warming of underlying layers in the photosphere, and hence to a modification of the atmospheric structure (‘line blanketing’: Kurucz 1979). The magnitude of the effect is roughly proportional to the ratio between line and continuum opacities, the latter being dominated by electron scattering in the atmospheres of hot stars. Thus line blanketing is approximately twice as effective in the electron-poor atmospheres of helium-rich stars as in the atmospheres of normal-composition stars. Consequently, the ultraviolet flux distribution of extreme helium stars is extremely sensitive to the effective temperature (Jeffery & Heber 1992; Dudley & Jeffery 1993).

Being rare and unusual, several extreme helium stars were observed within the first two years of operation of the *International Ultraviolet Explorer* (*IUE*: 1978–1979) and nearly all had been observed by the mid-1980s. Upon recognizing the great sensitivity of their fluxes to temperature, a series of second-epoch observations of extreme helium stars was made with *IUE* in the early 1990s.

1.3 Pulsation and cyclic changes

In the meantime it had been recognized that many extreme helium stars show photometric variability on time-scales of hours to weeks (e.g. Jeffery & Malaney 1985; Jeffery, Hill & Morrison 1986) and that the most luminous are likely to pulsate (Saio &

Jeffery 1988). Clearly, cyclic changes in flux due to pulsation would be as easy to measure but could mask any secular changes due to evolution. Such cyclic changes would, however, be extremely useful for measuring the temperature and radius variations associated with the pulsation and could, in conjunction with radial velocity measurements, help to ascertain the radius of a pulsating helium star, independently of its distance. Should the secular change be large compared with the cyclic change, then a measurement of the cyclic changes at one end of the secular vector would indicate the overall uncertainty in the length and direction of that vector.

Consequently, the second-epoch *IUE* observations of three extreme helium stars included observations repeated over an interval commensurate with their known time-scales for photometric variability. By good fortune, it was possible to obtain optical spectroscopy nearly simultaneously with these *IUE* data.

1.4 Objectives

In this paper, the *IUE* observations of extreme helium stars are described, the resulting angular diameters and effective temperatures are reported, and the time-dependent behaviour is considered.

2 IUE OBSERVATIONS

Table 1 records the journal of *IUE* observations of 17 extreme helium stars (EHes) used in this investigation. Approximately 150 low-resolution (LORES) spectra obtained with the Large Aperture (LAP) have been used, of which 78 were obtained by the principal author and 66 were obtained specifically for this investigation.

All of the images were retrieved directly from the *IUE* Final Archive (Nichols & Linsky 1996) as wavelength- and flux-calibrated files (MXLO images), thus avoiding inhomogeneities in the reduction of first-epoch observations (in particular) and taking advantage of the improved signal-to-noise ratio achieved in the Final Archive data products.

Wherever possible, pairs of images obtained with the Short Wavelength Prime (SWP) camera and either the Long Wavelength Reserve (LWR – early epochs) or the Long Wavelength Prime (LWP – later epochs) camera were identified. The principal criterion was that SW/LW pairs should have been obtained on the same date, but in a few cases – particularly first-epoch observations – this was not always achieved. In some cases, two images from the same camera were combined, using the exposure times to provide an appropriately weighted average spectrum. The SW and LW images were merged with relative weights of 100:1 (affecting the overlap region only) and trimmed to the wavelength range 1150–3350 Å.

3 SAAO OBSERVATIONS

By good fortune, time on the 1.9-m telescope at the South African Astronomical Observatory (SAAO) was awarded to two of the authors for entirely different programmes during 1995 May and roughly coincided with the period in which the *IUE* observations were scheduled. Spectroscopic observations of the *IUE* targets were obtained using the Image Tube Spectrograph and the Reticon Photon Counting System. All spectra were obtained in the blue region (3900–4500 Å) at a resolution of ~ 1 Å. A wavelength calibration spectrum was taken before and after each stellar observation. Spectra were background-subtracted, wavelength-calibrated,

Table 2. Radial velocity measurements v of extreme helium stars. JD' represents HJD-244 9800. Velocities are in km s^{-1} .

HD 168476		BD +1°4381		LS IV –1°2	
JD'	v	JD'	v	JD'	v
54.62	-174.0 ± 1.2	54.65	3.9 ± 1.8	54.63	-13.4 ± 3.6
55.57	-183.3 ± 1.1	55.65	4.4 ± 1.1	55.61	-14.6 ± 2.8
59.61	-172.3 ± 1.1	59.67	5.4 ± 1.5	59.64	-14.1 ± 2.4
60.61	-171.2 ± 1.1	60.67	4.6 ± 1.1	60.63	-16.1 ± 3.3
62.67	-169.1 ± 1.0			62.47	-13.0 ± 1.5
63.67	-164.7 ± 1.1			63.48	-17.1 ± 3.5
65.68	-169.2 ± 1.0	65.67	6.4 ± 1.5	65.51	-7.4 ± 1.3
66.52	-174.6 ± 1.3	66.54	5.6 ± 1.1	66.49	-10.4 ± 1.2
67.66	-166.0 ± 1.1	67.64	5.6 ± 1.5	67.49	-4.2 ± 1.7

linearized and normalized. Radial velocities were found by cross-correlation relative to a template spectrum – generally the best exposed spectrum of each star. The velocity shift and error were found by fitting a Gaussian to the peak of each cross-correlation function. The template velocities were obtained by cross-correlation relative to the radial velocity standards HD 80170, 121190, 121932, 157457, 203638 and 204867. All velocities were corrected to the heliocentric reference frame. Table 2 records the journal of velocities for each of three extreme helium stars used in this investigation.

4 ANALYSIS

Apparent flux from a stellar photosphere may be characterized by an effective temperature T_{eff} , an angular radius θ and an interstellar extinction coefficient E_{B-V} . The theoretical flux distribution of a helium star with a given temperature, $f_{\lambda, T_{\text{eff}}}$, may be computed using an appropriate model atmosphere (Jeffery & Heber 1992). The characteristic interstellar extinction $A_{\lambda, E_{B-V}}$ may be approximated using, for example, Seaton's (1979) law. Our initial goal was to determine T_{eff} , θ and E_{B-V} for each LW/SW observation in Table 1.

A grid of helium-rich model atmospheres was calculated covering the effective temperature range 6000–45 000 K. The composition of the models in this grid was chosen to be $n_{\text{H}} = 0$, $n_{\text{He}} = 0.99$, $n_{\text{C}} = 0.01$ and $[\text{Fe}] = 0.0$, reflecting a composition typical for extreme helium stars (Jeffery 1996) rather than one tailored specifically to each star observed. To be brutal, this choice was made to minimize computational effort – the alternative would have been to compute a complete grid for each star. However, the composition of several helium stars is still not well known, the amount of line blanketing included in the models remains incomplete, and the systematics of adopting the same model grid for every star are much more tractable. Therefore, the adoption of a single composition was the only sensible choice for a study of so many targets.

For this analysis, the grid was entirely rechecked and extended where necessary to cover the range of T_{eff} and $\log g$ measured for EHes in previous analyses (Fig. 1). In some cases, models could be computed close to the Eddington limit for a pure Thomson scattering atmosphere. For reasons that are not completely clear but are connected with the distribution of opacity, very low-gravity models would not converge at all T_{eff} .

Surface gravity affects the overall flux distribution through changes in the ionization balance and line broadening. The resolution of the spectrophotometry is insufficient to provide an independent constraint on $\log g$. Therefore previous measurements have been used to guide the construction of two sequences of

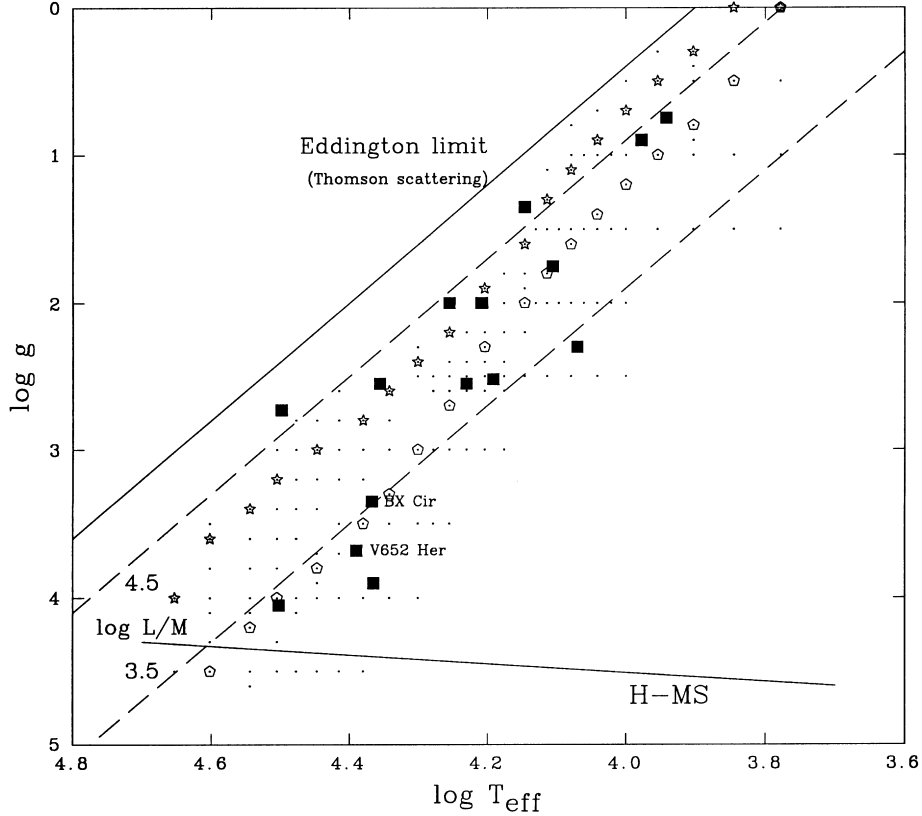


Figure 1. The grids of model atmospheres used in the least-squares measurement of T_{eff} . The low-gravity grid is shown by open stars, while the high-gravity grid is shown by open pentagons. The locations of EHeS measured in previous spectroscopic analyses (Table 5) are shown as filled squares. The complete grid of model atmospheres is indicated by black dots. The approximate locations of the Eddington limit (Thomson scattering), the hydrogen main-sequence and L/M contours are shown for reference. Two EHeS not studied in this paper are labelled.

model atmospheres with which the following procedure has been executed. These, together with previous measurements of EHeS, are shown in Fig. 1 and may be seen to represent a low- and a high-gravity sequence. They were chosen so that $\log g$ varies smoothly along each sequence and so that the combined sequence passes as close as possible to all EHeS in the sample.

These models were used to obtain best-fitting solutions for the observed IUE fluxes, essentially by residual minimization. A variety of approaches was investigated; only that which led to the final results presented here is described in detail. The principle was to fit the theoretical flux distribution

$$\phi_{\lambda, E_{B-V}, T_{\text{eff}}, \theta} = \theta^2 f_{\lambda, T_{\text{eff}}} A_{\lambda, E_{B-V}}$$

to the observed fluxes F_{λ} at the resolution given by the models ($\sim 20 \text{ \AA}$) using chi-squared minimization. In computing

$$\chi^2 = \sum_{\lambda} \frac{(F_{\lambda} - \phi_{\lambda})^2}{\sigma_{\lambda}^2},$$

σ_{λ}^2 are the variances of the binned fluxes. The errors associated with the best-fitting parameters x_i are given by the diagonal elements $(\alpha^{-1})_{ii}$ of the inverse of the covariance matrix α , whose elements are given by

$$\alpha_{ij} = \sum_{\lambda} \left(\frac{\partial \phi_{\lambda}}{\partial x_i} \frac{\partial \phi_{\lambda}}{\partial x_j} / \sigma_{\lambda}^2 \right).$$

Several χ^2 minimization procedures are capable of solving for x_i , here T_{eff} , θ and E_{B-V} . The final method adopted was the

downhill simplex method (Nelder & Mead 1965), implemented using a variant of the algorithm AMOEBA (Press et al. 1989). The method was proven to give identical results to an independently developed brute-force algorithm. The principal difference between our version of AMOEBA (Woolf & Jeffery 2000) and that published by Press et al. (1989) is that ours passes both the free parameters and the observed spectrum to the function to be minimized. In this case, the function is χ^2 (cf. CHISQ, Press et al. 1989). The brute-force procedure originally developed for this project (CRAWLER) entailed a cross-shaped grid with an adaptive mesh size that literally crawled across the χ^2 surface until it located a minimum. A coarse snapshot of the entire χ^2 surface verified that only one such minimum existed.

The value of E_{B-V} or, indeed, of T_{eff} obtained from χ^2 minimization to the IUE ultraviolet fluxes alone did not always agree with previous results or with expectation. One problem is that the simultaneous measurement of T_{eff} and E_{B-V} from the flux distribution alone is not always feasible – the solutions can be nearly degenerate. The measurement of E_{B-V} from the 2175- \AA feature alone is not helpful, since the interstellar feature coincides with a large number of temperature-sensitive metal lines in the photospheric spectrum. Hence a large reddening increases the strength of the interstellar feature and implies a high effective temperature with little metal line blocking, whilst a small reddening reduces the interstellar feature and implies a low effective temperature with more metal line blocking.

Visual and infrared photometry can provide additional constraints on T_{eff} and E_{B-V} . However, the use of data that were not

Table 3. Optical photometry of extreme helium stars.

Star	<i>V</i>	<i>B</i> − <i>V</i>	<i>U</i> − <i>B</i>	<i>V</i> − <i>R</i>	<i>R</i> − <i>I</i>	Reference
HD 124448	9.989	−0.093	−0.796			Jeffery & Lynas-Gray (1990)
HD 144941	10.130	+0.012	−0.534			Jeffery & Hill (1996)
HD 160641	9.825	+0.144	−0.802			Landolt (1986)
HD 168476	9.268	−0.012	−0.666			Landolt (1986)
HD 225642	10.307	+0.160	−0.754	+0.086	+0.092	Landolt (1986)
BD +37°1977	10.170	−0.242	−1.264	−0.141	−0.324	Jordi et al. (1991)
BD +10°2179	9.948	−0.191	−0.859			Landolt (1986)
BD +1°4381	9.557	+0.188	−0.536	+0.134	+0.107	Landolt (1986)
BD −1°3438	10.328	+0.460	−0.246			Landolt (1986)
BD −9°4395	10.535	+0.055	−0.833			Landolt (1986)
CoD −46°11775	11.22	+0.06				Heber, Jonas & Drilling (1986)
CoD −48°10153	11.483	+0.440	−0.318	+0.329	+0.306	Landolt (1986)
LSIV +6°2	12.17	−0.07				Drilling & Hill (1986)
LSIV −1°2	11.009	+0.375	−0.485	+0.264	+0.284	Landolt (1986)
LSIV −14°109	11.152	+0.331	−0.277	+0.298	+0.250	Landolt (1986)
LSS 4357	12.620	+0.412	−0.521	+0.288	+0.284	Landolt (1986)
LSS 5121	13.253	+0.316	−0.699	+0.212	+0.227	Landolt (1986)

contemporaneous with the *IUE* observations could have voided our search for variations. We therefore introduced a single set of *UBVRI* photometry (Table 3) to all spectra of the same star. An average E_{B-V} was thus obtained, together with preliminary values of T_{eff} and θ . At this point, the flux distribution fits were inspected manually and compared with previous determinations of T_{eff} and E_{B-V} . If these checks proved satisfactory, the automatic measurement of E_{B-V} was adopted. Otherwise, a value was estimated by obtaining the best fit between model and spectrum at all ultraviolet wavelengths including, in particular, the 2175-Å feature.

The adopted E_{B-V} was subsequently applied as a fixed value, the weights attached to the *UBVRI* photometry were reduced to a very low value and the solution for T_{eff} and θ was repeated. Consequently, the final relative measurements of these are dominated by the *IUE* data, whilst the average values and E_{B-V} are also constrained by the optical photometry.

Important sources of systematic error include anomalous interstellar extinction and differences in photospheric composition. CoD −46°11775=LSE 78 is a good example (Jeffery 1993) of the former. The 2175-Å feature corresponds with a region where the *IUE* camera sensitivity is low. Although our χ^2 reflects the signal-to-noise ratio (*S/N*) in the photometry, the minimization may still be influenced by systematic errors in the *IUE* calibration at low flux levels. Each case has been considered individually and carefully. In most cases E_{B-V} has been measured satisfactorily from the χ^2 minimization. In a few, the result contradicts other indicators, such as the optical spectrum, sufficiently that a compromise value of E_{B-V} has been adopted. Such cases are noted. The contribution of the composition was checked using a sequence of model atmospheres computed with $n_{\text{C}} = 0.003$. Where the raw data are of good quality, the systematic changes are small. For the lowest-gravity stars, T_{eff} increases by $\lesssim 1$ per cent for the coolest stars and negligibly for the hottest stars in the sample. For higher-gravity stars T_{eff} is reduced by ~ 5 per cent. Many of the cooler stars occupy the temperature domain where the effect of iron line blanketing on the flux distribution is most severe (Dudley & Jeffery 1993) and most are variable on comparatively short time-scales (see Section 7).

Improvements in the model atmospheres and simultaneous ultraviolet and optical (*UBVRI*) photometry would reduce many systematic effects.

The consistency of the solution can, in principle, be checked by comparing the integrated observed flux, after dereddening, with the integrated model flux in the same spectral region. This is equivalent to the comparison of T_{eff} with $T_{\text{mod}} = T_{\text{eff}}(\text{model})$ used by Drilling et al. (1984a). Algebraically, let

$$F = \int_{IUE} (F_{\lambda}/A_{\lambda}) d\lambda$$

and

$$\Phi = \int_{IUE} (\phi_{\lambda}/A_{\lambda}) d\lambda$$

be integrals over the wavelength region observed with *IUE*. If we make the approximation that the ratio of observed flux to total flux in both theoretical and physical stellar atmospheres is the same, then

$$F/\Phi \approx (T_{\text{eff}}/T_{\text{mod}})^4.$$

Without the approximation, we have

$$T_{\text{eff}}^4 - T_{\text{mod}}^4 = (F - \Phi)/\Phi\theta^2.$$

Thus, disregarding errors in θ , a 1 per cent discrepancy in the flux integral corresponds to a 4 per cent error in T_{eff} . The ratio F/Φ given in Table 4 thus gives an indication of where large systematic errors in the average values of T_{eff} and θ still exist. CoD −46°11775 illustrates this well.

Despite all precautions, significant discrepancies between the current and previously published measurements of T_{eff} remain. On an absolute scale, the previous values may often be preferred. However, the crucial observables in the present study are δT_{eff} and $\delta\theta$. Considerable care has been taken to minimize the impact of known systematic errors on these quantities. However, it is clear that this experiment is close to the limits of validity of the model atmospheres and of the photometry.

5 EFFECTIVE TEMPERATURES AND ANGULAR DIAMETERS

The results are shown in Table 4. Columns 1 and 2 give the star identifiers and the Julian date of each observation; the time difference between the SW and LW images is reflected in the number of significant figures. Columns 3 and 4 give the integrated *IUE* flux

$$F_{IUE} = \int_{1150}^{3350} F_{\lambda} d\lambda$$

and its standard deviation

$$\left(\int_{1150}^{3350} \sigma_{\lambda}^2 d\lambda \right)^{1/2}.$$

Columns 5 and 6 give, first, the adopted extinction E_{B-V} and standard error and, below, the effective temperature T_{eff} and standard error for each spectrum. Columns 7 and 8 give the angular radius for each spectrum. Column 9 gives the ratio F/Φ described above. Columns 10 to 13 give values for E_{B-V} , T_{eff} and θ from the previous analyses cited. Note that *only* the *IUE* spectrophotometry has been used in the measurements of T_{eff} and θ reported here. Fig. 2 shows one spectrum for each star analysed, dereddened by the adopted extinction E_{B-V} , together with the best-fitting theoretical flux distribution. Each star is discussed below.

HD 124448. Theoretical flux distributions reproduce *IUE* and *UBV* photometry well. Values of E_{B-V} and T_{eff} obtained from χ^2 minimization are in excellent agreement with previously published analyses.

HD 144941. Theoretical flux distributions reproduce the *IUE* photometry well, but do not fit the *B* and *V* photometry. T_{eff} is ~ 5000 K higher than that found spectroscopically. The star is not variable (Jeffery & Hill 1996), but is very metal-poor and comparatively hydrogen-rich (Jeffery & Harrison 1997; Harrison & Jeffery 1997). Although it is likely that problems are related to the photospheric composition, a sequence of model atmospheres with $n_{\text{H}} = 0.05$ did not resolve them. Self-consistent hydrogen-deficient model atmospheres with very low metallicities have not yet been developed.

HD 160641. The χ^2 minimization gave $E_{B-V} \sim 0.28\text{--}0.33$ with $T_{\text{eff}} \sim 22\,500$ K. The presence of strong C IV $\lambda 1550$ and He II $\lambda 1640$ absorption as well as previous analyses imply higher T_{eff} . Forcing a fit with E_{B-V} in the range 0.40–0.48 gives reasonable agreement between ultraviolet and *UBV* photometry except in the range 1800–2500 Å. Thorough examination demonstrates that the particular interstellar extinction around 2175 Å is significantly narrower than that given by Seaton’s (1979) law (Fig. 3). It is known that $\lambda 2175$ absorption varies considerably from one line of sight to another (Fitzpatrick & Massa 1988) and the problem is not uncommon amongst extreme helium stars and related objects (Jeffery 1995). This, together with insufficient resolution in the models around the UV resonance lines, degrades the quality of the fit. Since our goal is to measure relative changes in T_{eff} , we have adopted $E_{B-V} = 0.45$. We note that χ^2 is increased because of the systematic error introduced in the adopted extinction, and that the formal errors on the resulting T_{eff} and θ are correspondingly greater than those arising from photometric and model atmosphere errors alone.

HD 168476. Theoretical flux distributions reproduce *IUE* and

UBV photometry well. Values of E_{B-V} and T_{eff} obtained from χ^2 minimization are in excellent agreement with previously published analyses.

HD 225642. Theoretical flux distributions mostly reproduce *IUE* and *UBV* photometry well, with the exception of the short-wavelength end of the *IUE* long-wavelength camera. The *RI* fit is poor. The values of E_{B-V} and T_{eff} obtained from χ^2 minimization are in good agreement with one previous analysis.

BD +37°1977. With $E_{B-V} = 0.0$ and $T_{\text{eff}} \sim 40\,000$ K, the *IUE* and *UBVRI* photometry closely follow the Rayleigh–Jeans tail of the flux distribution. The only published measurement of T_{eff} predates *IUE* and contemporary model atmospheres.

BD +10°2179. Theoretical flux distributions reproduce the *IUE* photometry well, but not the *B* and *V* photometry. The star is not variable (Hill, Lynas-Gray & Kilkenny 1984; Grauer, Drilling & Schönberner 1984) and is metal-poor (Heber 1983). T_{eff} is probably too high as a consequence of the latter.

BD +1°4381. The χ^2 values for E_{B-V} and T_{eff} provide a good match to the *IUE* and *UBV* photometry. E_{B-V} and T_{eff} are similar to those previously reported from *IUE* measurements but T_{eff} is higher than measured spectroscopically. Systematic differences between spectroscopic and photometric measures of T_{eff} have been persistently difficult to resolve for EHes.

BD –1°3438. The χ^2 values for E_{B-V} and T_{eff} provide a good match to the *IUE* and *UBV* photometry. Although E_{B-V} is higher than previously reported, T_{eff} derived therefrom matches a recent spectroscopic measurement and is compensated for by a larger angular radius.

BD –9°4395. Theoretical flux distributions reproduce the *IUE* photometry well, but do not fit the *B* and *V* photometry.

CoD –46°11775. For wavelengths longer than 2000 Å, anomalous interstellar extinction has already been identified. E_{B-V} is therefore adopted from the analysis of Jeffery (1993), whereupon the *IUE* photometry longward of 2400 Å fits well. The *B* and *V* photometry are not well fitted; being similar to a mismatch in other stars of similar T_{eff} , this may be due to composition.

CoD –48°10153. The *IUE* data for this star are very noisy. χ^2 gives $E_{B-V} \sim 0.38\text{--}0.56$ with $T_{\text{eff}} \sim 10\,500$ K. Fixing $E_{B-V} = 0.45$ gives a reasonable fit to *IUE* and *UBV* photometry, with *R* and *I* being somewhat faint as in other EHes of similar T_{eff} .

LSIV +6°2. The χ^2 method gave $E_{B-V} = 0.16$ and $T_{\text{eff}} \sim 29\,000$ K, but the fit around 2175 Å was suspect due to *IUE* noise around 2000 Å. Eyeballing the fit for E_{B-V} gave theoretical flux distributions that reproduce *IUE* and *BV* photometry well and T_{eff} in good agreement with previously published analyses.

LSIV –1°2. Theoretical flux distributions reproduce *IUE* and *UBV* photometry well. The *RI* fit is poor. The values of E_{B-V} and T_{eff} obtained from χ^2 minimization are in reasonable agreement with previous analyses; attempting to reduce E_{B-V} reduces T_{eff} and substantially degrades the fit.

LSIV –14°109. The χ^2 minimization gives $E_{B-V} \sim 0.36\text{--}0.58$ as a consequence of low *S/N* in the *IUE* data. Adopting a mean value $E_{B-V} = 0.45$ gives a reasonable match between theoretical fluxes and *IUE* and *UBV* photometry with $T_{\text{eff}} \sim 8800$ K. Increasing E_{B-V} further causes substantial problems for the fit, although published values for T_{eff} suggest that this is desirable. Reducing $E_{B-V} = 0.40$ makes no substantial difference to the quality of fit.

LSS 4357. The *IUE* spectra are very noisy below 1500 Å and from 2000 to 2400 Å. Consequently χ^2 only constrains $E_{B-V} \sim 0.40\text{--}0.54$ and $T_{\text{eff}} \sim 13\,000\text{--}14\,000$ K, being ~ 2000 K lower than the spectroscopic value. To achieve $T_{\text{eff}} \sim 16\,000$ K requires

Table 4. The *IUE* measurements of effective temperature, angular diameter and interstellar extinction for extreme helium stars. The last four columns refer to previous work as cited. Fluxes are in $\text{erg s}^{-1} \text{cm}^{-2}$, temperatures in kelvins and angular diameters in radians. F/Φ is the ratio of measured to predicted flux in the *IUE* cameras.

Star	JD 244 0000	Current measurements							Previous measurements		Ref.	
		F_{IUE}	\pm	E_{B-V} T_{eff}	\pm	θ $\times 10^{-11}$	\pm	F/Φ	E_{B-V}	T_{eff}		θ $\times 10^{-11}$
HD 124448		$\times 10^{-9}$		0.11	0.01				0.08	15500 ± 500	5.2	Dri84
	3875.0	3.07	0.01	15654	146	5.57	0.19	1.01				
	4068.2	2.96	0.01	15793	166	5.41	0.22	1.03				
	9177.3	2.99	0.01	15831	142	5.35	0.12	1.01				
HD 144941		$\times 10^{-9}$		0.25	0.02				0.25	23200 ± 500		Har97
	4258.1	3.26	0.01	27819	906	3.33	0.14	0.998				
HD 160641 =V2076 Oph		$\times 10^{-9}$		0.45	0.02				0.40	31900 ± 1500	5.5	Dri84
	4050.9	3.24	0.01	29888	1669	6.01	0.21	0.92				
	4069.5	3.59	0.01	29216	1277	6.62	0.25	0.94				
	4460.3	3.21	0.02	29821	1578	5.95	0.24	0.90				
	5468.53	2.85	0.01	27733	1219	6.25	0.23	0.90				
	5468.58	2.74	0.01	28312	1384	5.99	0.23	0.91				
	5468.65	2.68	0.01	27808	1314	6.05	0.22	0.90				
	5468.69	2.70	0.01	27274	1116	6.27	0.21	0.90				
	5468.74	2.72	0.01	28029	1193	6.04	0.20	0.91				
	5468.79	2.76	0.01	28171	1242	6.06	0.20	0.91				
	9468.6	3.35	0.01	31802	1386	5.62	0.15	0.92				
HD 168476 =PV Tel		$\times 10^{-9}$		0.13	0.01				0.12	12400 ± 400	9.6	Dri84
	4068.1	2.20	0.02	12098	125	10.2	0.55	0.96				
	4318.2	2.10	0.01	12255	34	9.62	0.27	0.97				
	9176.6	2.39	0.01	12530	50	9.63	0.21	0.99				
	9839.5	2.23	0.01	12475	49	9.50	0.25	1.00				
	9843.0	2.17	0.01	12394	44	9.45	0.22	0.98				
	9847.5	2.24	0.01	12383	46	9.72	0.23	0.99				
	9852.5	2.26	0.01	12430	47	9.57	0.21	0.98				
	9856.6	2.21	0.01	12411	47	9.54	0.22	0.99				
	9860.0	2.33	0.01	12459	44	9.70	0.21	0.99				
	9865.6	2.28	0.01	12507	49	9.47	0.21	0.99				
HD 225642 =V1920 Cyg =LS II +33 5		$\times 10^{-9}$		0.31	0.02				0.22	15000 ± 500	5.7	Dri84
	4843.2	1.02	0.00	14668	273	7.20	0.30	0.90		16180 ± 500		Je98b
	9176.3	1.08	0.00	14942	211	7.20	0.19	0.93	0.33	20200		Heb86
BD +37°1977		$\times 10^{-8}$		0.00	0.01					50000		Wol74
	3659.4	2.21	0.01	36749	901	2.24	0.04	1.00				
	3813.2	2.21	0.01	39765	1530	2.09	0.06	1.02				
	3878.8	2.09	0.01	41226	888	1.97	0.04	1.02				
	4205.8	2.18	0.01	41251	1297	2.03	0.06	1.03				
	4354.5	2.15	0.01	42202	691	1.96	0.04	1.03				
	9467.7	2.20	0.01	42342	1017	1.99	0.03	1.04				
BD +10°2179		$\times 10^{-9}$		0.00	0.01				0.00	17700 ± 600	4.2	Dri84
	4205.8	6.19	0.02	19812	397	3.38	0.13	0.98				
	9467.6	6.11	0.02	19104	557	3.57	0.09	0.97				
BD +1°4381 =FQ Aqr		$\times 10^{-10}$		0.10	0.02				0.10	9500 ± 400	11.2	Dri84
	4068.5	6.65	0.06	9671	58	10.8	0.56	0.92		8270 ± 250		Pan00
	4068.6	6.85	0.05	9693	35	11.9	0.44	0.93				
	9177.5	6.48	0.03	9678	36	11.4	0.51	1.57				
	9839.6	7.13	0.04	9541	38	11.8	0.43	0.94				
	9843.6	7.12	0.04	9690	39	11.1	0.37	0.93				
	9847.6	6.82	0.03	9792	37	10.3	0.37	0.91				
	9852.6	6.32	0.03	9694	36	10.6	0.35	0.95				
	9856.5	6.32	0.03	9752	37	10.2	0.34	0.92				
	9860.6	6.39	0.02	9805	41	10.0	0.34	0.92				
	9865.5	6.62	0.03	9803	36	10.3	0.31	0.94				
BD -1°3438 =NO Ser		$\times 10^{-11}$		0.77	0.04				0.40	10900 ± 600	9.1	Dri84
	4065.2	8.04	0.02	10828	413	18.2	4.57	1.05		11750 ± 250		Pan00
	4068.7	8.56	0.01	10961	173	17.6	1.81	0.99				
	5116.2	9.26	0.01	11141	102	17.8	1.03	1.02				
	9468.7	9.61	0.01	11427	75	16.9	0.66	1.02				

Table 4 – continued

Star	JD 244 0000	Current measurements						Previous measurements			Ref.		
		F_{IUE}	\pm	E_{B-V}	\pm	θ $\times 10^{-11}$	\pm	F/Φ	E_{B-V}	T_{eff}		θ $\times 10^{-11}$	
BD $-9^{\circ}4395$ =V2205 Oph		$\times 10^{-9}$		0.24	0.02				0.30	23000 ± 700	4.0	Dri84	
	4068.3	1.59	0.01	19824	800	3.92	0.21	1.01		22700 ± 1200		Jef92	
	4070.7	1.61	0.01	19770	472	4.00	0.15	1.03					
	9176.4	1.73	0.01	21238	373	3.67	0.07	1.04					
CoD $-46^{\circ}11775$ =LSE 78		$\times 10^{-10}$		0.25	0.06				0.10	13600 ± 400	3.4	Dri84	
	4458.6	5.76	0.02	19406	3922	2.80	0.41	0.62	0.25	18000 ± 700		Jef93	
	4838.0	6.04	0.03	19324	4194	2.96	0.45	0.65	0.25	23300		Heb86	
	9468.7	5.98	0.02	20161	3238	2.81	0.26	0.68					
CoD $-48^{\circ}10153$ =V354 Nor =LSS 3378		$\times 10^{-11}$		0.45	0.04				0.35	9400 ± 500	6.7	Dri84	
	4069.6	6.06	0.09	11114	253	5.46	0.66	0.88					
	4840	4.86	0.06	9677	120	7.59	0.44	0.88					
LSIV $+6^{\circ}2$	7640.4	$\times 10^{-10}$	9.93	0.03	31886	1157	1.31	0.03	1.05	0.22	31800 ± 800	1.3	Jef98a
LSIV $-1^{\circ}2$ =V2244 Oph		$\times 10^{-10}$		0.50	0.02					0.45	11900 ± 400	7.1	Dri84
	4468.7	1.22	0.01	12187	90	7.62	0.39	1.05		12750 ± 250		Pan00	
	9466.7	1.30	0.01	12119	58	7.77	0.22	0.99					
	9839.7	1.32	0.01	12248	58	7.66	0.24	1.00					
	9843.7	1.28	0.01	12147	62	7.55	0.24	0.96					
	9847.7	1.32	0.01	11991	78	7.98	0.28	0.96					
	9852.7	1.28	0.01	12184	79	7.56	0.26	0.97					
	9856.7	1.33	0.01	12222	72	7.74	0.23	1.00					
LSIV $-14^{\circ}109$		$\times 10^{-11}$		0.45	0.05					0.20	8400 ± 500	7.5	Dri84
	4459.9	5.39	0.08	8938	324	10.3	1.04	0.95		9500 ± 250		Pan00	
	5116.4	5.35	0.05	8877	154	10.4	0.76	0.94					
	9469.7	5.55	0.04	8869	113	10.8	0.44	0.90					
LSS 4357		$\times 10^{-11}$		0.45	0.04					0.60	18700		Heb86
	5235	3.82	0.04	12876	430	3.24	0.32	0.88		16130 ± 500		Jef98b	
	7640.2	4.85	0.02	13048	169	3.27	0.15	0.77					
LSS 5121	7640.0	$\times 10^{-11}$	6.36	0.02	29772	1830	1.67	0.05	0.97	0.61	28300		Heb86

References: Dri84=Drilling et al. (1984a,b); Har97=Harrison & Jeffery (1997); Heb86=Heber et al. (1986); Jef92=Jeffery & Heber (1992); Jef93=Jeffery (1993); Jef98a=Jeffery (1998); Jef98b=Jeffery et al. (1998); Pan00=Pandey et al. (2000); Wol74=Wolff et al. (1974).

$E_{B-V} \geq 0.60$. In default of a good ultraviolet spectrum, we report the χ^2 solution.

LSS 5121. The *IUE* data are noisy, and $\text{Ly}\alpha$ was excluded from the χ^2 fit. The latter gave $E_{B-V} = 0.40$ and $T_{\text{eff}} = 19\,179\text{ K}$, in contradiction to the optical spectrum (Heber, Jonas & Drilling 1986) and the presence of strong $\text{C IV } \lambda 1550$ and $\text{He II } \lambda 1640$ absorption. Adopting $E_{B-V} = 0.65$ gave T_{eff} more in keeping with the latter, although noisy photometry in the range 2000–2500 Å gives the impression that E_{B-V} should be lower.

6 SECULAR VARIABILITY

Saio (1988) calculated equilibrium models for luminous helium stars with degenerate carbon–oxygen cores and helium envelopes. From these, contraction rates for shell-burning helium stars can be obtained as a function of mass and effective temperature. Surface gravities and effective temperatures have already been measured for most of the stars in the current sample. These give the L/M ratio and, using a theoretical mass–luminosity relation (Jeffery 1988), one estimate of the total mass (Table 5).

The first object of this investigation was to compare measurements of helium star effective temperatures, obtained over a 10–15 yr baseline, with the contraction rates predicted by Saio (1988). The effective temperatures of extreme helium stars for which at

least two *IUE* measurements have been given in Table 4 are shown as a function of time in Fig. 4. The panel for each star also shows the predicted change (Saio 1988) in T_{eff} for 0.7- and 0.9- M_{\odot} helium stars over a 10-yr baseline, assuming the mean T_{eff} measured here for each star. Note that the contraction rates for 0.7- M_{\odot} stars are an order of magnitude smaller than for 0.9- M_{\odot} stars and are barely different from zero on the scale of Fig. 4.

BD $+1^{\circ}4381$, CoD $-48^{\circ}10153$ and LSIV $-14^{\circ}109$. For all 0.7- M_{\odot} models and for 0.9- M_{\odot} models with $T_{\text{eff}} \leq 12\,000\text{ K}$, the predicted contraction rates are mostly negligible compared with the measurement errors. These stars all have $T_{\text{eff}} \leq 12\,000\text{ K}$ and no detectable change in T_{eff} or θ , in agreement with the predictions.

LSIV $-1^{\circ}2$ and BD $-1^{\circ}3438$. For the two remaining cool EHes, the predicted 0.9- M_{\odot} contraction rate is non-negligible. LSIV $-1^{\circ}2$ shows no detectable change. The T_{eff} of BD $-1^{\circ}3438$ has risen by a few hundred degrees between 1979 and 1994. Although the change might be accounted for by short-term variations and photometric errors, it may be significant. Pandey et al. (2000) find a high surface gravity for this star, which would contradict a high contraction rate. However, it is also variable (Kilkenny et al. 1999a) on a time-scale comparable with strange-mode pulsations seen in luminous EHes, but not in high-gravity EHes (Saio & Jeffery 1988).

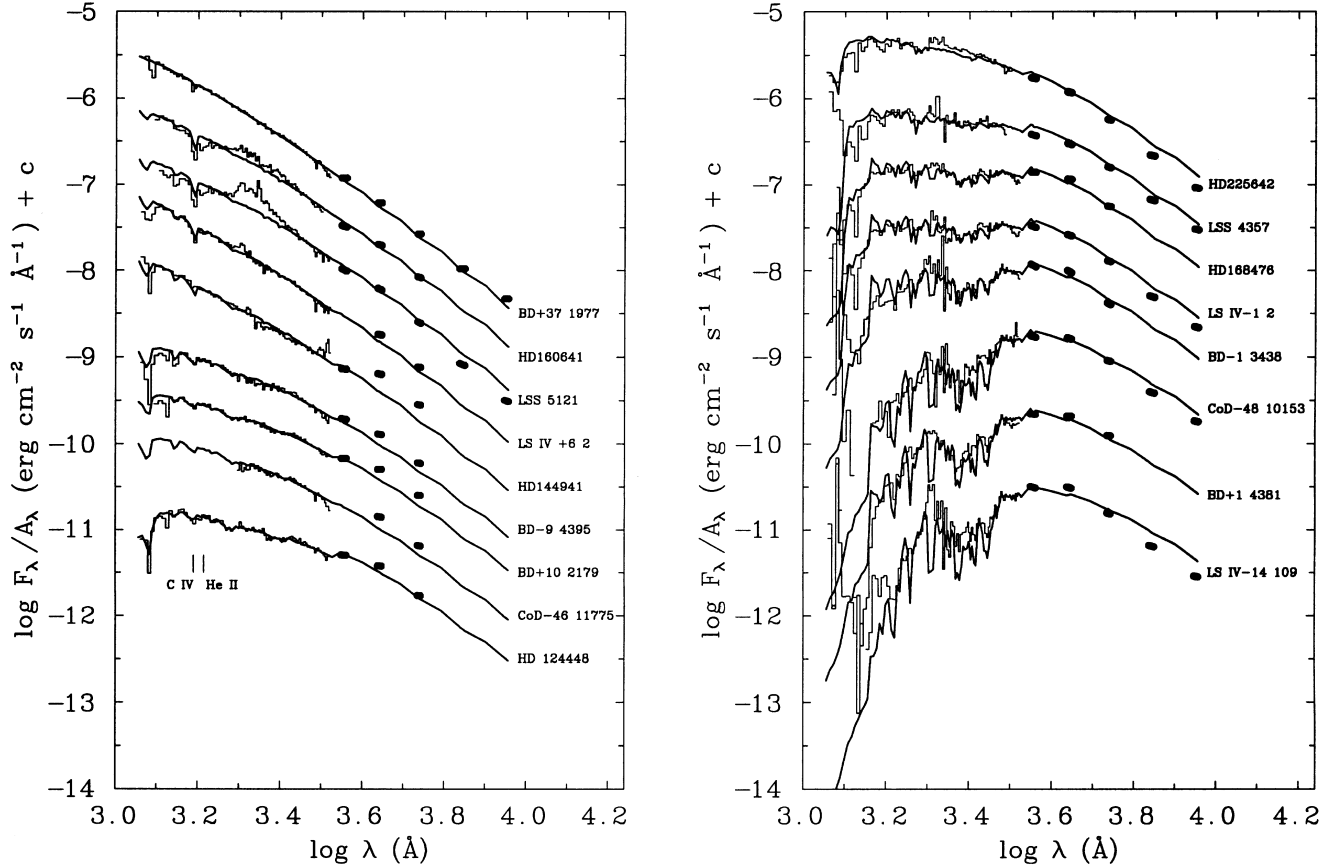


Figure 2. One SW/LW pair of *IUE* spectra for each programme star, binned to the resolution of the model atmosphere grid (thin histogram), together with the photometry from Table 3 (solid points), is compared with the theoretical flux distributions (thick curve) that best fit the *IUE* spectra. The spectra have been dereddened by the amount shown in Table 4 and multiplied by an arbitrary constant. The *IUE* and model spectra correspond to the last entry for each star in Tables 1 and 4.

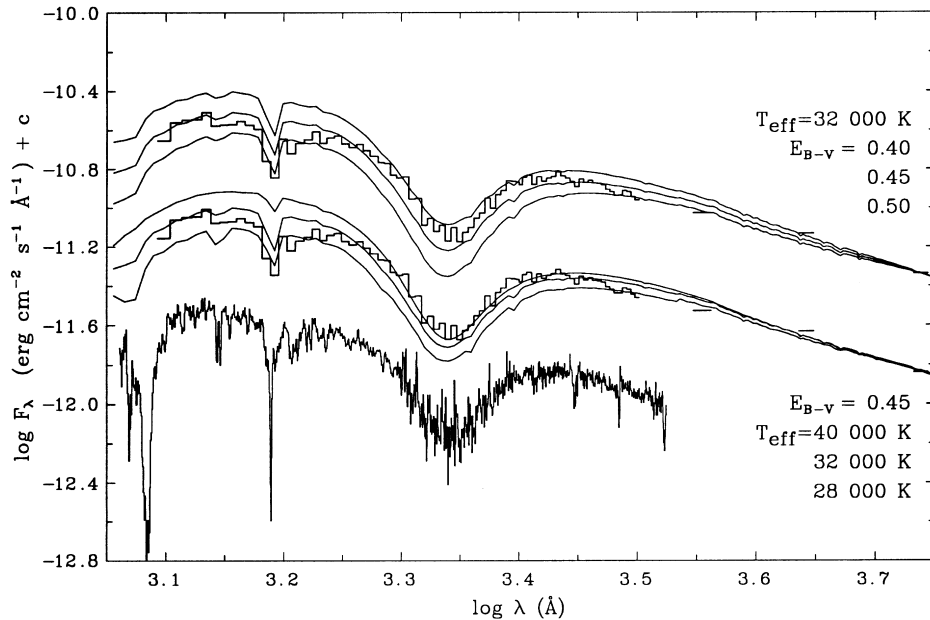


Figure 3. The combined *IUE* spectrum of HD 160641 for JD 244 9468.6 (bottom) together with flux distributions for model atmospheres with $T_{\text{eff}} = 28, 32$ and 40 kK (middle) and reddened using Seaton's (1979) law with $E_{B-V} = 0.40, 0.45$ and 0.50 (top). The models are plotted over the binned and offset *IUE* data and, in this case, normalized at the mean *V* magnitude. Note that no combination of T_{eff} and E_{B-V} simultaneously fits the entire flux distribution.

Table 5. Spectroscopic mass estimates for extreme helium stars obtained from self-consistent surface gravity and effective temperature measurements and from the core mass–shell luminosity relation for helium shell-burning stars (Jeffery 1988). Measurement errors lead to mass errors substantially in excess of $0.1 M_{\odot}$ in all cases. The main purpose of this table is to demonstrate the likely relative masses of extreme helium stars.

Star	$\log T_{\text{eff}}$	$\log g$	M/M_{\odot}	Reference
HD 124448	4.192	2.52	0.57	Sch74
HD 144941	4.365	3.9	0.49	Har97
HD 160641	4.50	2.73	1.05	Lyn87
HD 168476	4.14	1.35	0.95	Wal81
HD 225642	4.209	2.00	0.71	Jef98b
BD +10°2179	4.23	2.55	0.59	Heb83
BD +1°4381	3.94	0.75	0.80	Pan00
BD −1°3438	4.07	2.30	0.53	Pan00
BD −9°4395	4.36	2.55	0.74	Jef92
CoD −46°11775	4.26	2.00	0.81	Jef93
LS IV +6°2	4.502	4.05	0.53	Jef98a
LS IV −1°2	4.106	1.75	0.66	Pan00
LS IV −14°109	3.977	0.90	0.79	Pan00
LSS 4357	4.207	2.00	0.70	Jef98a

References: Har97 = Harrison & Jeffery (1997); Heb83 = Heber (1983); Jef92 = Jeffery & Heber (1992); Jef93 = Jeffery (1993); Jef98a = Jeffery (1998); Jef98b = Jeffery et al. (1998); Lyn87 = Lynas-Gray et al. (1987), based on T_{eff} and L ; Pan00 = Pandey et al. (2000); Sch74 = Schönberner & Wolf (1974); Wal81 = Walker & Schönberner (1981).

HD 124448, BD +37°1977 and BD +10°2179. These show no evidence for a significant increase in T_{eff} during the *IUE* lifetime. In the cases of HD 124448 and BD +10°2179 at least, the surface gravities are high and indicate relatively low luminosities and masses, $\leq 0.6 M_{\odot}$ (Table 5). The possibility that BD +10°2179 could be cooling due to a secular expansion cannot be excluded. The early evolution of a helium star may include a relatively rapid expansion phase (e.g. Weiss 1987).

HD 225642, CoD −46°11775 and LSS 4357. These have a low surface gravity and could have been expected to show measurable contraction. In these cases the data quality and quantity are too poor to draw any conclusion.

HD 160641, HD 168476 and BD −9°4395. These are all low-surface-gravity EHes. Accordingly, their masses are expected to exceed $0.7 M_{\odot}$ and their contraction rates should be observable, as appears to be the case.

It could be argued that short-term variations could account for all of the changes seen in HD 160641, HD 168476, BD −9°4395 and BD −1°3438. All are luminous helium stars unstable against strange-mode pulsation instability (Jeffery et al. 1985; Lynas-Gray et al. 1987; Saio & Jeffery 1988; Kilkenny et al. 1999). However, HD 160641 and 168476 have been monitored with *IUE* over intervals comparable with their natural oscillation frequencies. The amplitude of their short-term variations – at least in T_{eff} – appears to be small compared with the secular change reported here.

To confirm that the observed heating is due to a secular contraction, the effective temperatures from Table 4 are also shown as a function of angular radius in Fig. 5. Vectors represent the contraction at constant luminosity of a $0.9 M_{\odot}$ model over the

interval covered by the *IUE* observations. In all four cases, the observed heating is consistent with an overall contraction.

It may be argued that contraction rates computed from equilibrium models, which ignore time-dependent terms in the structure equations, are unrepresentative. For example, if previous evolution had led the helium star to be overluminous, then the contraction rate would exceed the Saio (1988) value as the star attempted to recover equilibrium. In fact, this could ultimately be to advantage because, if contraction rates are sensitive to past evolution and if they can be measured with sufficient precision, they could provide a test for stellar evolution models.

Meanwhile, there is reasonable evidence that, in up to four cases, *IUE* measurements have led to the direct detection of helium star evolution and that the contraction rates detected are comparable with conservative predictions. No large secular changes have been identified that were not predicted, with the exception of the possible expansion of BD +10°2179. The heating rates indicated for HD 160641, HD 168476, BD −9°4395 and BD −1°3438 are approximately 120, 20, 95 and 33 Kyr^{-1} respectively. The heating rates predicted for a $0.9 M_{\odot}$ helium star with the same T_{eff} are 105, 50, 108 and 30 Kyr^{-1} .

7 CYCLIC VARIABILITY

Several studies of extreme helium stars have attempted to identify periodic behaviour in their photometry and radial velocities, with mixed success. There is good theoretical and empirical evidence that the variations are caused by pulsations, but attempts to define definitive periods and light curves have been largely unsuccessful. The exceptions are V652 Her and BX Cir, which, with short periods and low luminosities, are discussed extensively elsewhere (Lynas-Gray et al. 1984; Kilkenny et al. 1999b).

Reasonably well-studied variables include:

- HD 160641 = V2076 Oph (Lynas-Gray et al. 1987);
- HD 168476 = PV Tel (Walker & Hill 1985; Jones et al. 1989; Lawson et al. 1993);
- HD 225642 = V1920 Cyg (Morrison & Willingale 1987);
- BD +1°4381 = FQ Aqr (Jeffery & Malaney 1985; Jeffery et al. 1986; Lawson et al. 1993; Kilkenny et al. 1999a);
- BD −1°3438 = NO Ser (Jeffery et al. 1986; Lawson et al. 1993; Kilkenny et al. 1999a);
- BD −9°4395 = V2205 Oph (Jeffery et al. 1985);
- CoD −48°10153 = V354 Nor = LSS 3378 (Lawson et al. 1993);
- LS IV −1°2 = V2244 Oph (Morrison 1987; Jones et al. 1989; Lawson et al. 1993).

There is some evidence for variability in:

- LS IV +6°2 (Jeffery 1998; Lawson & Kilkenny 1998);
 - LSS 4357 (Lawson & Kilkenny 1998);
 - CoD −46°11775 = LSE 78 (Lawson & Kilkenny 1998);
 - LS IV −14°109 (Lawson et al. 1993).
- There is no evidence for variability in:
- HD 124448 (Jeffery & Lynas-Gray 1990);
 - HD 144941 (Jeffery & Hill 1996);
 - BD +10°2179 (Hill et al. 1984; Grauer et al. 1984).

Of the variables, HD 160641 and BD −9°4395 have complex light curves, which have been attributed to multiperiodic and non-radial oscillations. For the remainder, the time-scales (or ‘periods’) reported for the variations are relatively close to those

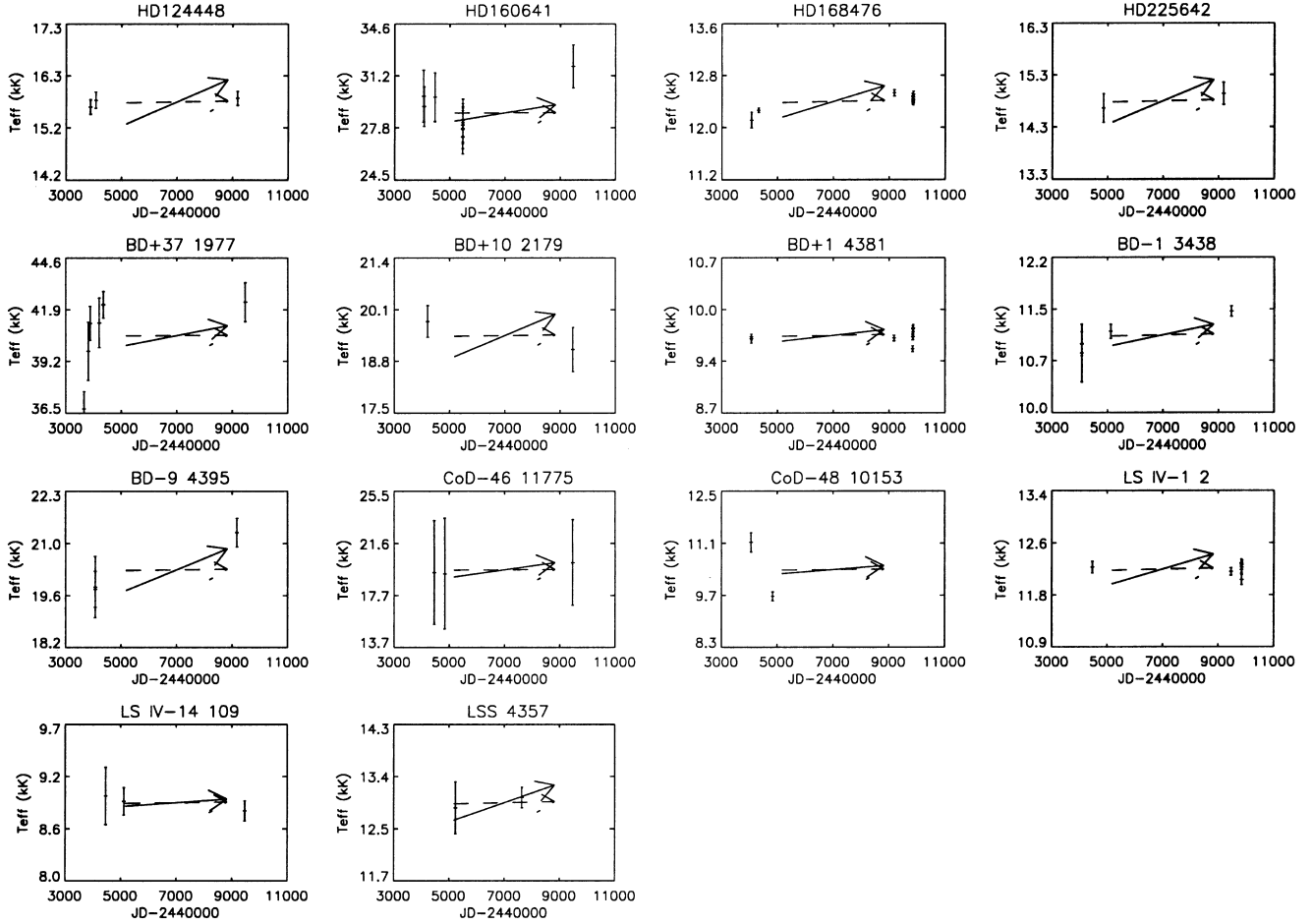


Figure 4. The effective temperature measurements of all helium stars with two or more *IUE* spectra from Table 4 are shown as a function of Julian date. The vectors shown in each panel represent the temperature change predicted by Saio (1988) for shell helium-burning stars of $0.7 M_{\odot}$ (dashed) and $0.9 M_{\odot}$ (solid) and T_{eff} similar to that shown. The vertical error bars represent the error given in Table 4; the horizontal marks are simply locators.

expected from radial pulsation theory (Saio & Jeffery 1988). Lawson et al. (1993) find that the luminosity and radial velocity curves for BD +1°4381 are correctly phased for the variation to be due to radial pulsation.

Adopting the hypothesis that at least some of the extreme helium star variables are radial pulsators, *IUE* was used to measure T_{eff} and θ variations over at least one pulsation cycle of the three most accessible candidates. These were HD 168476, BD +1°4381 and LS IV -1°2, which have been reported to show ‘periods’ of approximately 9, 20 and 11 d respectively (see references above). The *IUE* observations were taken during seven shifts in 1995 May, spaced out to cover the longest period. Figs 7 to 9 show the ultraviolet and radial velocity behaviour. Variability is evident in all three stars.

Ascribing a period to the variations is difficult. It is noted that from 5 yr of observations, Kilkenny et al. (1999a) failed to identify a unique period for either BD +1°4381 or BD -1°3438 that persisted for more than one season. It appears from their light curves (e.g. Jones et al. 1989; Lawson et al. 1993; Kilkenny et al. 1999a) that extreme helium star variations are not regular. In the case of extremely non-adiabatic pulsations anticipated in the highly extended envelopes of luminous helium stars, it may be that the pulsations become highly chaotic.

Whatever the long-term properties of the pulsations, it seems

reasonable here to characterize short-term behaviour by a local time-scale. One might adopt, for example, the interval between successive light maxima. Here we have made the simplifying and probably wrong assumption that, over the small interval represented by the 1995 data, the variations can be approximated by a sine function with a single period (Π). We have attempted to identify the best-fitting sine function for each data set (T_{eff} , θ , F_{IUE} and radial velocity v). In each case the mean, amplitude and phase are free parameters. Our initial approach was to minimize χ^2 for as many solutions as possible within reasonable constraints.

The results are illustrated for each star in Fig. 6, which shows χ^2 for each of the T_{eff} , θ , F_{IUE} and v solutions as a function of trial period. The χ^2 values are normalized to their maximum value in the period range plotted. Since the data are sparse and of finite duration, the interpretation of these plots is non-trivial. Any solution with a trial period similar to twice the sampling interval is likely to be spurious – these are indicated by a dotted line in the plots. Trial periods long compared with the duration of the observations also lead to spuriously small χ^2 . Each variable shows a number of other χ^2 minima, but generally not at the same period. Consistency checks (e.g. $F_{IUE} \propto \theta^2 T_{\text{eff}}^4$) eliminate some of these. Pursuing each trial-period solution through to estimates of various stellar dimensions eliminates others; the resultant stellar masses are also shown in Fig. 6, for example.

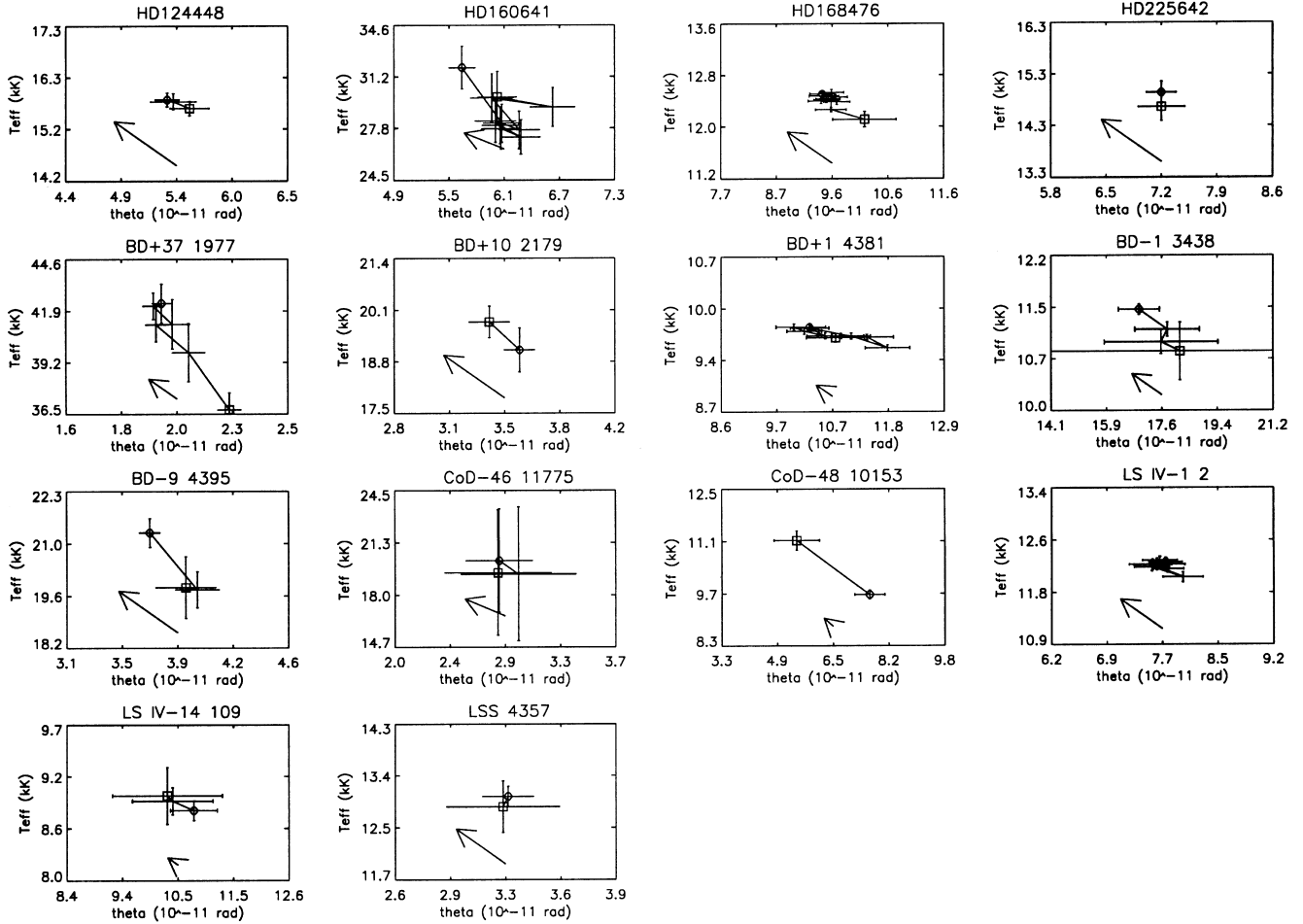


Figure 5. The same data as for Fig. 4 except that Julian date is replaced by angular radius θ . The *first* datum in each sequence is marked by a square, the last by a circle. The evolution vectors are shown only for the 0.9- M_{\odot} case, and have a length corresponding to the predicted *contraction* over the interval covered by the observations. Errors in both T_{eff} and θ are shown.

The adopted solutions for T_{eff} , θ , F_{IUE} and v are shown in Figs 7 to 9 and in Table 6. The periods finally adopted for HD 168476 and LS IV $-1^{\circ}2$ (see Table 6) are based on the minimum χ^2 for angular radius and previous estimates of their periods (Jones et al. 1989). The period for BD $+1^{\circ}4381$ is an estimate based on roughly twice that expected from early observations (Jeffery & Malaney 1985), but roughly comparable with some of the values reported by Kilkenney et al. (1999a). Shorter periods (e.g. 15 d) lead to self-contradictory results.

Figs 7 to 9 demonstrate a number of important results. First, the product $\theta^2 T_{\text{eff}}^4$, which represents the total luminosity variation of the star, is in phase with and has nearly the same amplitude as the total flux measured by *IUE*, as expected. Secondly, θ and T_{eff} are precisely out of phase so that maximum T_{eff} corresponds with minimum radius, as is also expected. For a radially pulsating star, it is further expected that, for a strictly sinusoidal oscillation, minimum radius should precede minimum radial velocity by ~ 0.25 cycles. Fig. 6 demonstrates the phase difference $\Delta\phi = \phi(v_{\text{min}}) - \phi(\theta_{\text{min}})$ as a function of period. HD 168476 and BD $+1^{\circ}4381$ show $\Delta\phi \sim 0.25$ over the relevant period range. LS IV $-1^{\circ}2$ does not, but in all cases the solutions for v are far from optimal. It is evident that the adoption of any period to fit an incomplete ensemble of data such as these is probably dangerous. However, it does enable us to estimate the *amplitudes* of the

variations in a quantitative way – it is these which are of primary interest to us here.

An independent verification of these periods and amplitudes can be obtained from Lawson et al. (1993), who published radial velocities obtained in 1991 with comparable equipment over a comparable interval (20 d). Optimum least-squares solutions to these data are shown in Fig. 10 and in Table 6. The velocity amplitude for HD 168476 is consistent between 1991 and 1995, whilst the 1995 amplitudes for the other two stars are roughly half the 1991 amplitudes. The periods obtained for these 1991 data are not the same as those found for our 1995 observations, in line with the photometric results (Kilkenney et al. 1999a,b).

8 STELLAR RADII, DISTANCES AND MASSES

If a star is pulsating radially, the variation in its angular radius $\delta\theta$ is related to the variation in its actual radius δR through the relation

$$\frac{\delta R}{R} = \frac{\delta\theta}{\theta}.$$

Since $\delta\theta$ and θ have already been measured and δR may be obtained by integrating the radial velocity, R should be

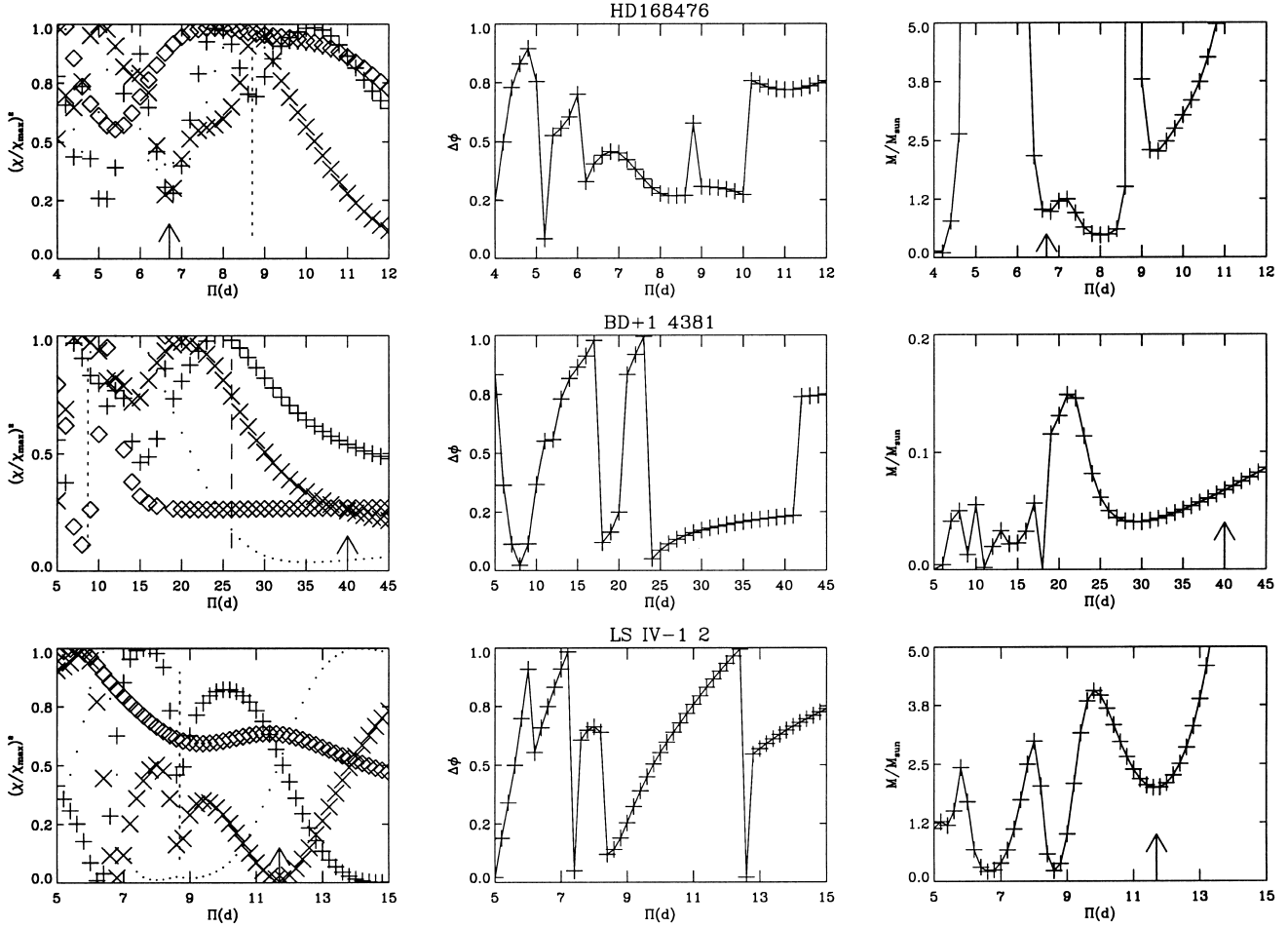


Figure 6. Identifying pulsation periods for variable helium stars. The left-hand panels show the normalized χ^2 for T_{eff} (+), θ (\times), F_{IUE} (\cdot) and v (\diamond) as a function of trial period Π for each star. The adopted period is marked by a vertical arrow. Twice the mean IUE sampling interval is marked by a vertical dotted line. The duration of the data set is marked by a vertical dashed line (BD +1^o4381 only). The centre and right-hand panels show the phase difference $\Delta\phi$ between θ and v and the derived stellar mass M , respectively, as a function of Π for each star. Computed solutions are connected by straight lines. Adopted periods are again shown by arrows.

immediately available. Ideally, R should be obtained using high-precision simultaneous data with good time resolution. In particular, such data should allow for (e.g.) non-sinusoidal behaviour. For the relatively faint early-type long-period low-amplitude variables considered here, suitable data are very difficult to acquire. In addition, EHe pulsators may increasingly be thought of as irregular pulsators (e.g. Kilkeny et al. 1999a), so that only simultaneous multiwavelength measurements of individual pulsation cycles can provide a definitive result. On the other hand, the least-squares solutions obtained above provide a cycle-averaged measurement of the variations. The radial semi-amplitude δR is given by the integral of the velocity solution,

$$\delta R = \frac{f\Pi\delta v}{2\pi}$$

where f transforms the observed radial velocity into the stellar rest frame, allowing for spherical projection and limb darkening. Conventionally, $f = 1.31$ (Parsons 1972), but recent work (Montañés Rodríguez & Jeffery 2000) indicates that $f \approx 1.41$ is better for small-amplitude pulsators.

With semi-amplitudes δR and $\delta\theta$ and the mean angular radius θ , it is then trivial to obtain the stellar radius R and distance d . The

luminosity L follows from the mean T_{eff} already derived (Table 6) and, with a spectroscopic measurement of the surface gravity g (Table 5), the stellar mass M can also be obtained.

The results given in Table 6 are reasonable for HD 168476, marginal for LSIV -1^o2 and quite unrealistic for BD +1^o4381. The stellar radius (and hence mass) derived from our least-squares solutions to θ and v is strongly period-dependent (Fig. 6). For HD 168476 and LSIV -1^o2, the radius has a minimum close to the adopted period, so that Table 6 effectively reports minimum radii and masses for these two stars.

The measured T_{eff} and R for HD 168476 and LSIV -1^o2 are very similar, and the difference in mass arises entirely from the higher gravity of LSIV -1^o2 (Pandey et al. 2000). Our SAO spectra for these two stars are almost identical at the resolution and S/N obtained. Profiles of the gravity-sensitive diffuse He I lines (singlet and triplet) are virtually indistinguishable (Fig. 11). If T_{eff} is the same for both stars, then $\log g$ should be virtually identical. If we take $\log g = 1.35 \pm 0.25$ for LSIV -1^o2, then we obtain $M = 0.79 \pm 0.46 M_{\odot}$, in good agreement with the mass measured for HD 168476.

The result for BD +1^o4381 is more difficult to understand, in particular the very low and unlikely mass ($0.07 \pm 0.04 M_{\odot}$). The

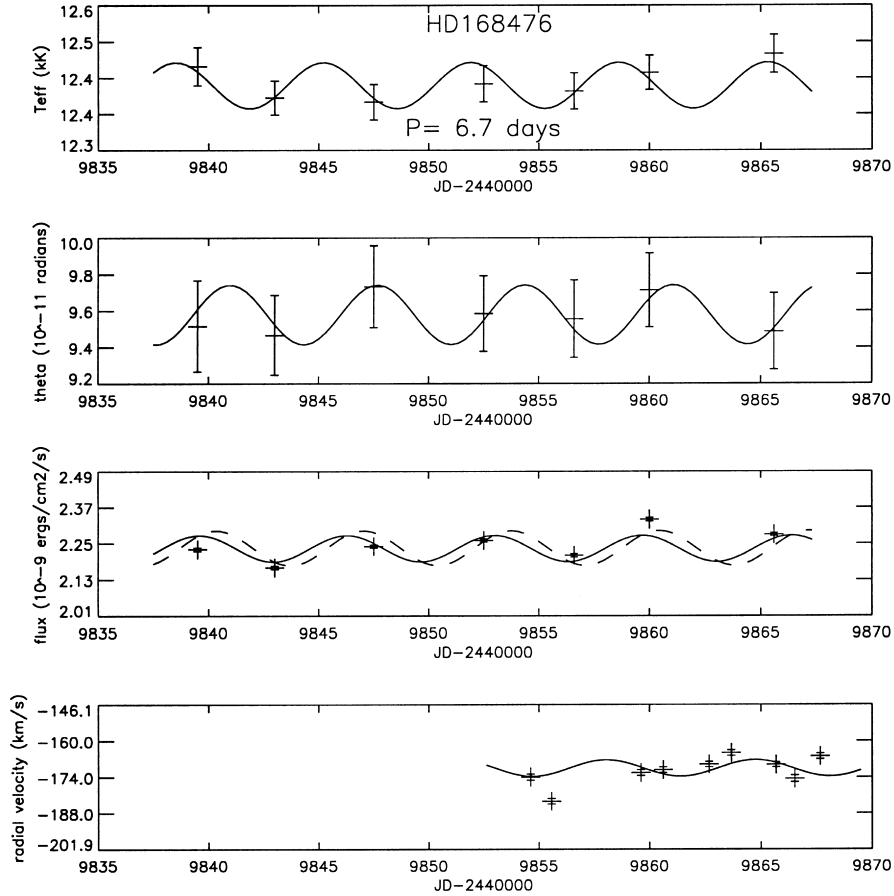


Figure 7. The ultraviolet and radial velocity behaviour of HD 168476=PV Tel during a 25-d observing run with *IUE* and the SAAO 1.9-m telescope in 1995. From top to bottom, the four panels show the variation of T_{eff} , θ , F_{IUE} and radial velocity reported in Tables 2 and 4. Superimposed on each is a sine curve; the period for all four fits is indicated in the top panel. The phase and amplitude were obtained from an independent least-squares fit to each set of data (solid curves). In the case of F_{IUE} , the dashed curve represents the product of the fits $\theta^2 T_{\text{eff}}^4$ scaled to the same mean value as F_{IUE} .

adopted period is approximately twice that expected, but comparable with some of the values reported by Kilkenny et al. (1999a). Pulsating extreme helium stars share several characteristics of RV Tauri stars, believed to be luminous post-asymptotic giant branch (AGB) stars. The latter show a variety of period changes, including period doubling, and light curves with alternating deep and shallow minima (Percy 1993). There are reasonable grounds to postulate that the oscillations shown by PV Tel variables should resemble the RV Tauri variables. Therefore, there does not seem to be a serious problem with Π . Reducing Π to a value in the range 10–20 d does not ameliorate the problem. With the similar amplitudes in v and θ , the radius is halved and the mass quartered.

What else could be wrong? The gravity ($\log g = 0.75$) given by Pandey et al. (2000) could be low. A factor of 10 increase would bring the measured mass up to $0.6 M_{\odot}$. At the same time the mass from the core mass–shell luminosity relation would be reduced from 0.80 to $0.53 M_{\odot}$. However, the reduction in luminosity would place the star below the pulsational instability boundary (Saio & Jeffery 1988), so the measured gravity is unlikely to be the problem.

The measured radius ($18.2 \pm 4.2 R_{\odot}$) is just over half that of HD 168476 and LS IV $-1^{\circ}2$. However, being some 2000 K cooler than LS IV $-1^{\circ}2$, BD $+1^{\circ}4381$ would have to have a radius some 66 per cent larger in order to have the same luminosity. Either δR

(and by implication δv) is too small, or $\delta\theta/\theta$ is too large. Since the 1995 velocity measures cover less than one-half of the pulsation cycle, $\delta v = 1.02 \text{ km s}^{-1}$ could be underestimated. The 1991 observations (Lawson et al. 1993) give $\delta v = 2.47 \text{ km s}^{-1}$, but with $\Pi = 18.5 \text{ d}$, the integral for δR is similar for both data sets. The alternative is that $\delta\theta$ is overestimated. The fits to the *IUE* measurements (Fig. 8) are not ideal. Whilst F_{IUE} is reasonably convincing, T_{eff} and θ are less satisfactory – even if the fit to θ does pass through the formal error bars of all the data. Of the three stars considered here, BD $+1^{\circ}4381$ is the coolest and has negligible flux in the *IUE* SW range. Despite the sensitivity of the *IUE* LW fluxes to T_{eff} the wavelength range may simply be too short to allow θ and T_{eff} to be measured truly independently. Regrettably, more than 80 nights of *UBV* photometry of BD $+1^{\circ}4381$ obtained in 1995 by Kilkenny et al. (1999a) do not overlap the period during which the *IUE* observations were made.

Table 7 compares mass estimates for three PV Tel variables. Spectroscopy and the core mass–shell luminosity relation (Jeffery 1988) provide the spectroscopic mass M_s . Photometric pulsation ‘periods’ and linear pulsation theory (Saio & Jeffery 1988) provide a pulsation mass M_p . Angular diameter and radial velocity measurements provide a direct mass M_d . It cannot be purely coincidence that three different methods lead, in at least two cases, to mass estimates that are in surprisingly good agreement,

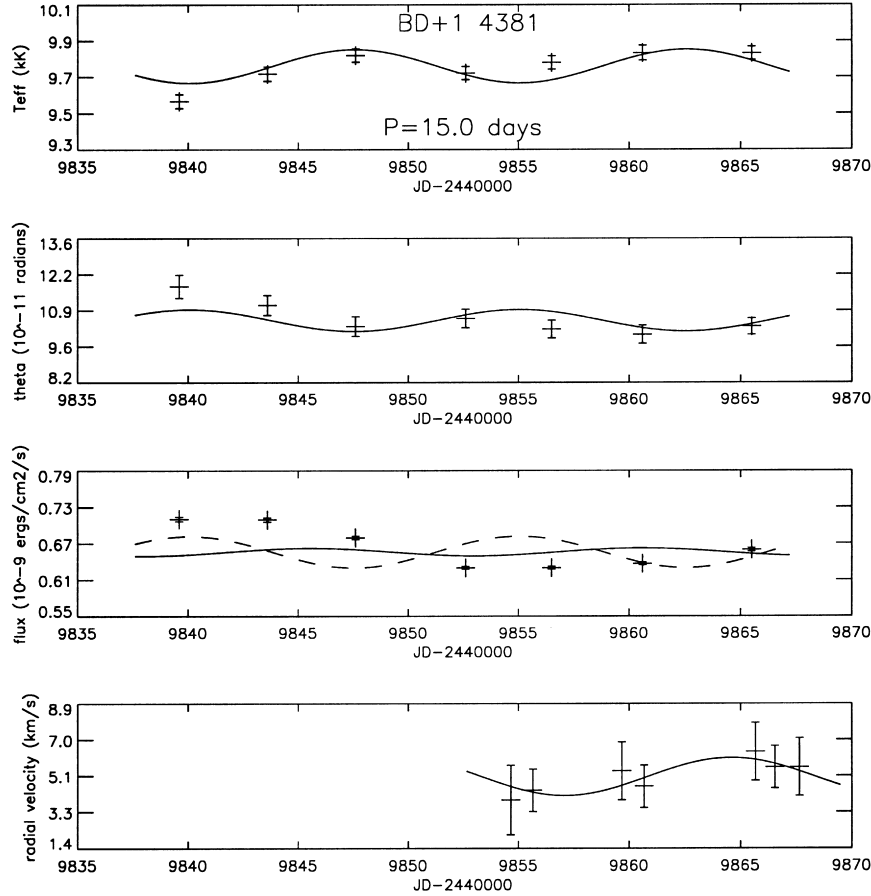


Figure 8. As Fig. 7 but for BD +1°4381 = FQ Aqr.

Table 6. Details of the least-squares solutions adopted for pulsating helium stars. ‘ δ ’ represents semi-amplitudes.

Star	HD 168476 =PV Tel	BD +1°4381 =FQ Aqr	LS IV -1°2 =V2244 Oph
Best-fitting solutions			
Π/d	6.7	40	11.7
$100\delta T_{\text{eff}}/T_{\text{eff}}$	0.48 ± 0.02	0.85 ± 0.02	0.77 ± 0.03
$100\delta\theta/\theta$	1.73 ± 0.18	6.26 ± 0.18	3.19 ± 0.32
$100\delta F_{IUE}/F_{IUE}$	1.98 ± 0.05	7.15 ± 0.41	1.96 ± 2.29
$\delta v/\text{km s}^{-1}$	3.147 ± 0.004	1.02 ± 0.23	3.04 ± 0.07
$\Delta\phi(v - \theta)$	0.55 ± 0.01	0.23 ± 0.08	0.89 ± 0.01
T_{eff}/K	12425 ± 47	9714 ± 38	12152 ± 27
Derived properties ($f = 1.41$)			
R/R_{\odot}	33.9 ± 3.6	18.2 ± 4.2	31.1 ± 3.2
d/kpc	8.00 ± 0.85	3.82 ± 0.87	9.08 ± 0.94
$\log L/L_{\odot}$	4.40 ± 0.06	3.43 ± 0.12	4.28 ± 0.06
$\log g$ (cgs) ^a	1.35 ± 0.15	0.75 ± 0.25	1.75 ± 0.25
M/M_{\odot}	0.94 ± 0.68	0.068 ± 0.044	1.99 ± 1.16
$\Delta\Pi/d \Rightarrow 1.2R$	0.2	6.9	1.0
1991 velocities			
Π/d	9.5	18.5	10.9
$\delta v/\text{km s}^{-1}$	3.53 ± 0.96	2.47 ± 4.36	7.07 ± 0.28

^a See Table 5 for references.

especially taking the numerous probable sources of error into consideration.

In order to make a significant improvement on these results, new measurements of radial velocity and angular diameter will

Table 7. Mass estimates (in M_{\odot}) for PV Tel variables from spectroscopy (M_s , Table 5), pulsation periods (M_p , Saio & Jeffery 1988) and direct measurement (M_d , Table 6).

Star	M_s	M_p	M_d
HD 168476 = PV Tel	0.95	0.85	0.94
BD +1°4381 = FQ Aqr	1.09	0.93	0.07
LS IV -1°2 = V2244 Oph ^a	0.66	0.94	1.99
LS IV -1°2 = V2244 Oph ^b	0.78	0.94	0.79

^a $\log g = 1.75$ (Pandey et al. 2000).

^b $\log g = 1.35$ – see text.

have to achieve better simultaneity and improved phase coverage with a precision at least as high as that achieved here. In the case of BD +1°4381 at least, simultaneous visual photometry will be necessary.

9 CONCLUSIONS

This investigation set out to test hypotheses that (a) the evolution of extreme helium stars would lead, in some cases, to changes in T_{eff} that would be observed on a time-scale of ~ 10 yr and (b) the pulsations of extreme helium stars would allow their masses to be measured directly.

Over 150 *IUE* spectra of 17 extreme helium stars have been combined to provide 70 SW/LW pairs covering 16 yr of *IUE* operation. These provide data suitable for studying long-term

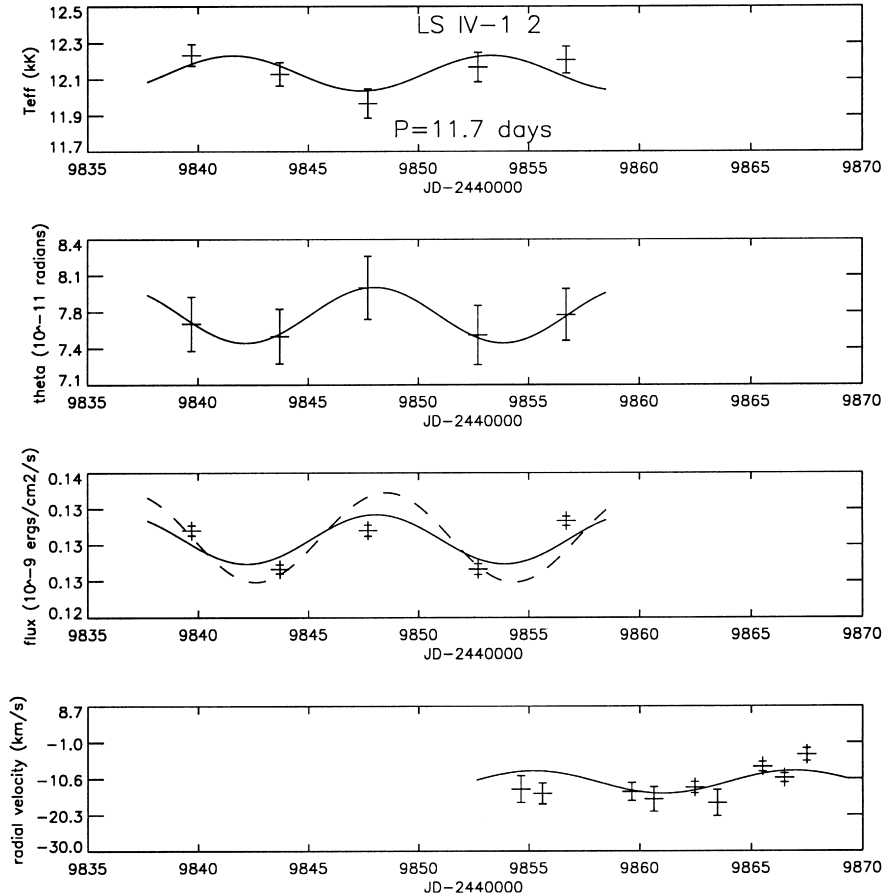


Figure 9. As Fig. 7 but for LSIV $-1^{\circ}2 = V2244$ Oph.

(>10 yr) changes in 12 stars and to study short-term variability (≤ 30 d) in four stars.

Using a grid of hydrogen-deficient model atmospheres, a χ^2 minimization method was devised to solve for effective temperature (T_{eff}) and angular radius (θ) for each *IUE* pair.

The long-term behaviour of T_{eff} was compared with the predictions of relatively simple stellar structure theory. If a star with a limited reserve of nuclear fuel shines with a certain luminosity, and neglecting other sources of energy, it will contract at a calculable rate. Values computed by Saio (1988) for extreme helium stars of 0.7 and $0.9 M_{\odot}$ were used in this comparison.

For extreme helium stars with low L/M ratios (high surface gravities), no change in T_{eff} was predicted or detected. For four stars with higher L/M ratios, temperature increases of between 20 and 120 K yr^{-1} were detected. The corresponding rates predicted for $0.9 M_{\odot}$ helium stars are between 30 and 110 K yr^{-1} , whilst they are negligible for $0.7 M_{\odot}$ stars. Consequently, there is now good evidence that some extreme helium stars are helium shell-burning giants contracting towards the white dwarf sequence with masses of up to $\sim 0.9 M_{\odot}$.

IUE spectrophotometry of three extreme helium stars known to be variable on a time-scale of days was used to establish periods and amplitudes of the variations in terms of T_{eff} and θ . Near-simultaneous radial velocity measurements enabled their radii and distances to be measured directly. Together with measurements of T_{eff} and surface gravity, the luminosities and masses follow. Although there are difficulties in defining the pulsation periods

Π and obtaining the correct phase between θ and radial velocity v , the overall results for two stars (HD 168476 and LS IV $-1^{\circ}2$) are excellent. Masses $\sim 0.8\text{--}0.9 M_{\odot}$ are indicated, in good agreement with stellar structure and pulsation theory. The radius for BD $+1^{\circ}4381$ appears to be badly underestimated by this method, possibly because its low T_{eff} makes it an unsuitable target for *IUE*.

In this study, both the contraction rate and mass of one star, HD 168476 = PV Tel, have been measured directly. For the first time these provide a single complete picture of an extreme helium star with a mass of $\sim 0.9 M_{\odot}$. It is contracting towards the white dwarf sequence, with T_{eff} increasing by $\sim 20 \text{ K yr}^{-1}$. As the prototype of the PV Tel variables, it pulsates, slightly irregularly, with $\Pi \sim 6\text{--}10$ d and a radius variation $\delta R \sim \pm 2$ per cent. Whilst other PV Tel variables may show larger amplitudes, HD 168476 would make an ideal target for intensive study on both long and short time-scales.

ACKNOWLEDGMENTS

The work reported in this paper is based on observations obtained with the *International Ultraviolet Explorer (IUE)* and recovered from the *IUE* Final Archive, and on observations obtained at the South African Astronomical Observatory (SAAO).

This research has been supported by the Northern Ireland Departments of Education and of Culture, Arts and Leisure through a grant to the Armagh Observatory; and by the UK

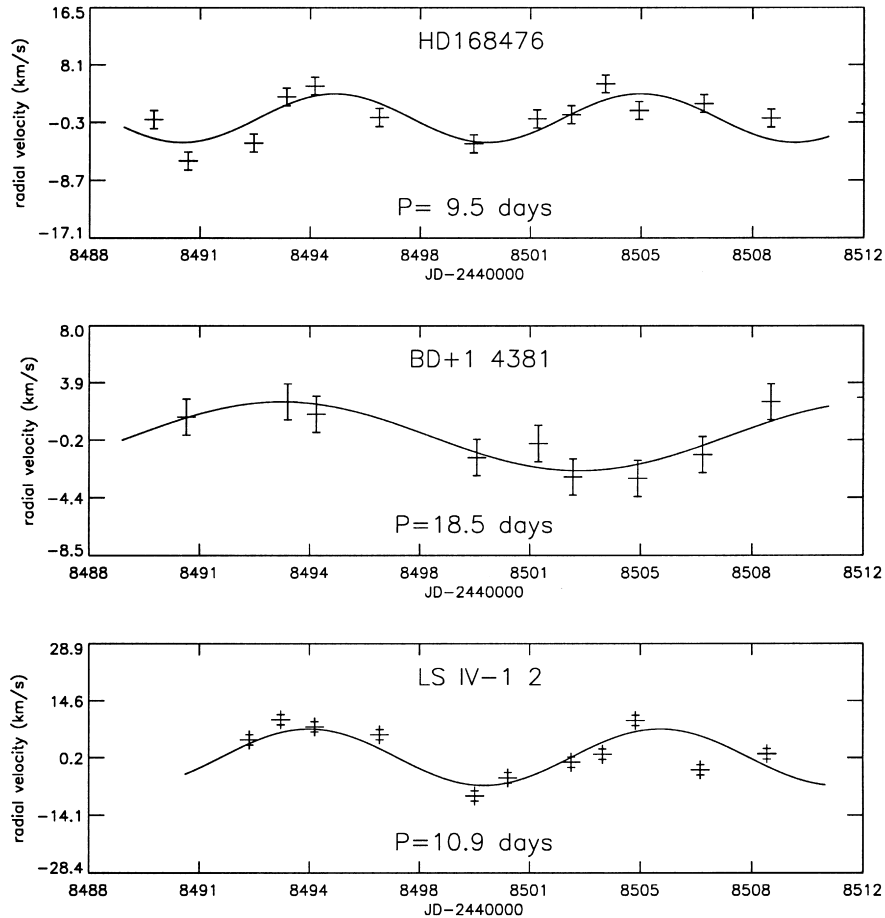


Figure 10. Least-squares solutions for radial velocities obtained in 1991 (Lawson et al. 1993).

Particle Physics and Astronomy Research Council Grant Number PPA/G/S/1998/00019. The referee, Dr A. E. Lynas-Gray, precipitated major improvements to the rigour of the paper and the quality of the conclusions.

NOTES ADDED IN PROOF

Note 1

During the revision of this manuscript, a paper by Massa & Fitzpatrick (2000) was published in which the authors demonstrate that some of the systematic errors still present in the *IUE* NEWSIPS data can be significantly reduced from around the 10 per cent level to ~ 3 per cent. While offering an algorithm for applying these corrections to existing NEWSIPS data products, they go on to propose that a rederivation of the NEWSIPS intensity transfer functions (ITF) would remove the remaining errors.

On reading the paper, the present authors had to decide between scrapping their entire *IUE* data set and starting again, or completing the analysis in its current form. Meanwhile, 25 snapshot orbits on the *Hubble Space Telescope* have been awarded in Cycle 8 for third-epoch ultraviolet spectrophotometry of most of the targets discussed in this paper. Observations will probably be obtained during late 2000 and 2001. Thus it was decided to proceed with the unmodified NEWSIPS data in this paper, leaving refinement to a future date when both new observations and improved NEWSIPS ITFs are available.

Note 2

The authors have been reminded that Heber & Schönberner (1981) concluded from a statistical study of the temperature distribution of 12 objects that extreme helium stars evolve to higher effective temperatures and finally cool down to become white dwarfs.

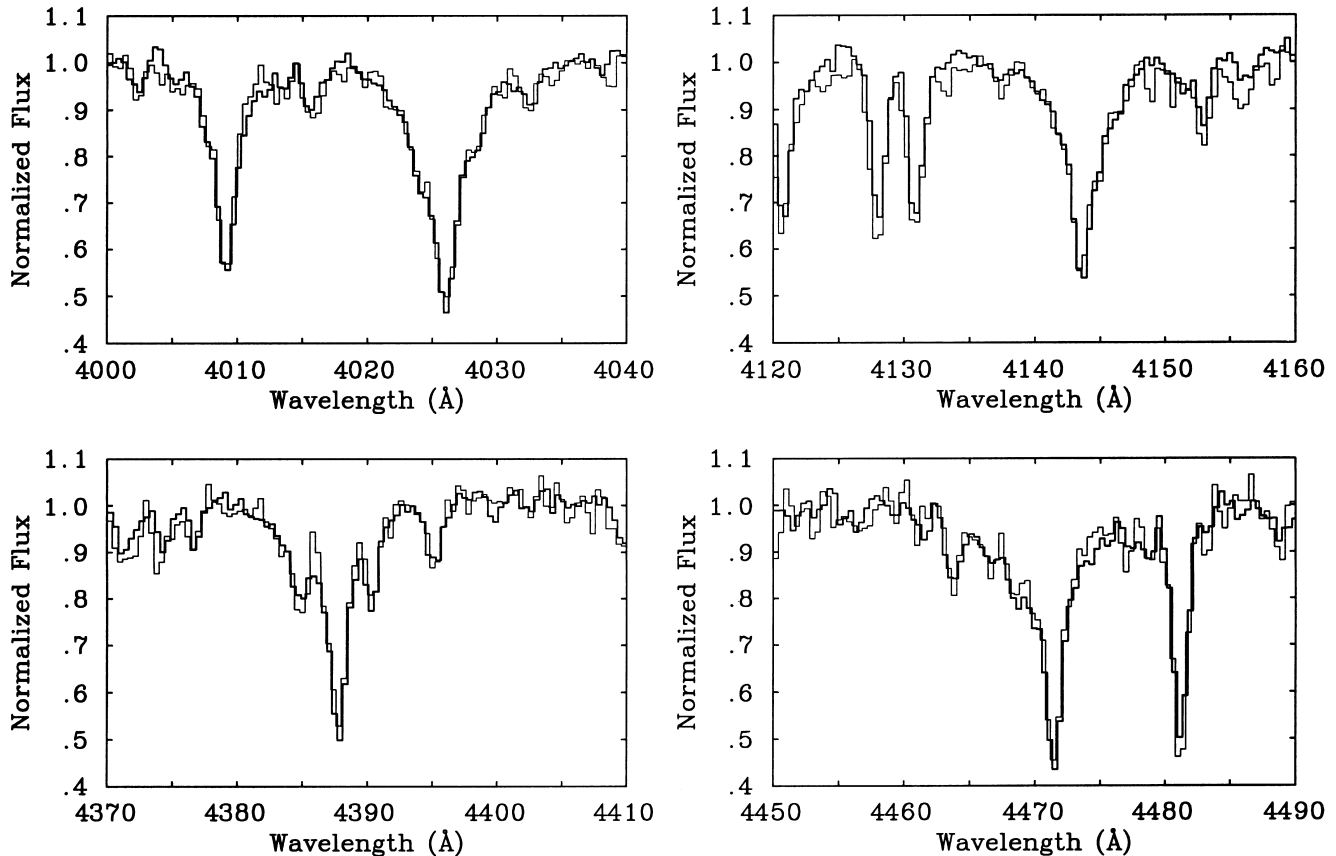


Figure 11. SAO spectra for HD 168476 (bold) and LSIV $-1^{\circ}2$ (light) comparing gravity-sensitive neutral helium line profiles at 4009, 4026, 4144, 4388 and 4471 Å. The spectra have been flux-normalized and velocity-shifted.

REFERENCES

- Drilling J. S., Hill P. W., 1986, in Hunger K., Schönberner D., Rao N. K., eds, IAU Coll. 87, Hydrogen-Deficient Stars and Related Objects. Reidel, Dordrecht, p. 499
- Drilling J. S., Schönberner D., Heber U., Lynas-Gray A. E., 1984a, *ApJ*, 278, 224
- Drilling J. S., Landolt A. U., Schönberner D., 1984b, *ApJ*, 279, 748
- Dudley R. E., Jeffery C. S., 1993, *MNRAS*, 262, 945
- Duerbeck H. W., Benetti S., Gautschy A., van Genderen A. M., Kemper C., Liller W., Thomas T., 1997, *AJ*, 114, 1657
- Fitzpatrick E. L., Massa D., 1988, *ApJ*, 328, 734
- Grauer A. D., Drilling J. S., Schönberner D., 1984, *A&A*, 133, 285
- Harrison P. M., Jeffery C. S., 1997, *A&A*, 323, 177
- Heber U., 1983, *A&A*, 118, 39
- Heber U., Jonas G., Drilling J. S., 1986, in Hunger K., Schönberner D., Rao N. K., eds, IAU Coll. 87, Hydrogen-Deficient Stars and Related Objects. Reidel, Dordrecht, p. 67
- Heber U., Schönberner D., 1981, *A&A*, 102, 73
- Hill P. W., Jeffery C. S., 1996, in Jeffery C. S., Heber U., eds, Hydrogen Deficient Stars, ASP Conf. Ser., Vol. 96. Astron. Soc. Pac., San Francisco, p. 395
- Hill P. W., Lynas-Gray A. E., Kilkeny D., 1984, *MNRAS*, 207, 823
- Iben I., Jr., 1984, *ApJ*, 277, 333
- Iben I., Jr., Tutukov A., 1985, *ApJS*, 58, 661
- Iben I., Jr., Kaler J. B., Truran J. W., Renzini A., 1983, *ApJ*, 264, 605
- Jeffery C. S., 1988, *MNRAS*, 235, 1287
- Jeffery C. S., 1993, *A&A*, 279, 188
- Jeffery C. S., 1995, *A&A*, 299, 135
- Jeffery C. S., 1996, in Jeffery C. S., Heber U., eds, Hydrogen Deficient Stars, ASP Conf. Ser., Vol. 96. Astron. Soc. Pac., San Francisco, p. 152
- Jeffery C. S., 1998, *MNRAS*, 294, 391
- Jeffery C. S., Harrison P. M., 1997, *A&A*, 323, 393
- Jeffery C. S., Heber U., 1992, *A&A*, 260, 133
- Jeffery C. S., Hill P. W., 1996, *Observatory*, 116, 156
- Jeffery C. S., Lynas-Gray A. E., 1990, *MNRAS*, 242, 6
- Jeffery C. S., Malaney R. A., 1985, *MNRAS*, 213, 61P
- Jeffery C. S., Skillen I., Hill P. W., Kilkeny D., Malaney R. A., Morrison K., 1985, *MNRAS*, 217, 701
- Jeffery C. S., Hill P. W., Morrison K., 1986, in Hunger K., Schönberner D., Rao N. K., eds, IAU Coll. 87, Hydrogen-Deficient Stars and Related Objects, ASP Conf. Ser., Vol. 96. Reidel, Dordrecht, p. 95
- Jeffery C. S., Hamill P. J., Harrison P. M., Jeffers S. V., 1998, *A&A*, 340, 476
- Jones K., van Wyk F., Jeffery C. S., Marang F., Shenton M., Hill P. W., Westerhuys J., 1989, *SAAO Circ.*, 13, 39
- Jordi C., Figueras J. M., Rosselló G., Torra J., 1991, *A&AS*, 87, 229
- Kilkeny D., Lawson W. A., Marang F., Roberts G., van Wyk F., 1999a, *MNRAS*, 305, 103
- Kilkeny D., Koen C., Jeffery C. S., Hill N. C., O'Donoghue D., 1999b, *MNRAS*, 310, 119
- Kurucz R. L., 1979, *ApJS*, 40, 1
- Landolt A. U., 1986, in Hunger K., Schönberner D., Rao N. K., eds, IAU Coll. 87, Hydrogen-Deficient Stars and Related Objects, ASP Conf. Ser., Vol. 96. Reidel, Dordrecht, p. 51
- Lawson W. A., Kilkeny D., 1998, *Observatory*, 118, 1
- Lawson W. A., Kilkeny D., van Wyk F., Marang F., Pollard K., Ryder S. D., 1993, *MNRAS*, 265, 351
- Lynas-Gray A. E., Schönberner D., Hill P. W., Heber U., 1984, *MNRAS*, 209, 387

- Lynas-Gray A. E., Kilkenny D., Skillen I., Jeffery C. S., 1987, *MNRAS*, 227, 1073
- Massa D., Fitzpatrick E. L., 2000, *ApJS*, 126, 517
- Montañés Rodríguez P., Jeffery C. S., 2000, *A&A*, submitted
- Morrison K., 1987, *MNRAS*, 224, 1083
- Morrison K., Willingale G. P. H., 1987, *MNRAS*, 228, 819
- Nelder J. A., Mead R., 1965, *Comput. J.*, 7, 308
- Nichols J. S., Linsky J. L., 1996, *AJ*, 111, 517
- Pandey G., Rao N. K., Lambert D. L., Jeffery C. S., Asplund M., 2000, *MNRAS*, submitted
- Parsons S. B., 1972, *ApJ*, 174, 57
- Percy J. R., 1993, *Ap&SS*, 210, 123
- Press W. H., Flannery B. P., Teukolsky S. A., Vetterling W. T., 1989, *Numerical Recipes: The Art of Scientific Computing*. Cambridge Univ. Press, Cambridge
- Saio H., 1988, *MNRAS*, 235, 203
- Saio H., 1993, *MNRAS*, 260, 465
- Saio H., 1995, *MNRAS*, 277, 1393
- Saio H., Jeffery C. S., 1988, *ApJ*, 328, 714
- Saio H., Jeffery C. S., 2000, *MNRAS*, 313, 671
- Schönberner D., 1975, *A&A*, 44, 383
- Schönberner D., Wolf R. E. A., 1974, *A&A*, 37, 87
- Seaton M. J., 1979, *MNRAS*, 187, 73p
- Seitter W. C., 1987, *Messenger*, 50, 14
- Walker H. J., 1985, *A&A*, 152, 58
- Walker H. J., Hill P. W., 1985, *A&AS*, 61, 303
- Walker H. J., Schönberner D., 1981, *A&A*, 97, 291
- Webbink R. F., 1984, *ApJ*, 277, 355
- Weiss A., 1987, *A&A*, 185, 165
- Wolff S. C., Pilachowski C. A., Wolstencroft R. D., 1974, *ApJ*, 194, L83
- Wood P. R., Faulkner D. J., 1973, *ApJ*, 181, 147
- Woolf V. W., Jeffery C. S., 2000, *A&A*, 358, 1001

This paper has been typeset from a \TeX/L\AA\TeX file prepared by the author.